

# Large detrital zircon data set investigation and provenance mapping: Local versus regional and continental sediment sources before, during, and after Ancestral Rocky Mountain deformation

Tyson M. Smith<sup>1,†</sup>, Joel E. Saylor<sup>2</sup>, Tom J. Lapen<sup>1</sup>, Ryan J. Leary<sup>3</sup>, and Kurt E. Sundell<sup>4,§</sup>

<sup>1</sup>Department of Earth and Atmospheric Sciences, University of Houston, Houston, Texas 77204, USA

<sup>2</sup>Department of Earth, Ocean, and Atmospheric Sciences, University of British Columbia, Vancouver, British Columbia V6T1Z4, Canada

<sup>3</sup>Department of Earth and Environmental Sciences, New Mexico Tech, Socorro, New Mexico 87801, USA

<sup>4</sup>Department of Geosciences, University of Arizona, Tucson, Arizona 85721, USA

## ABSTRACT

The increasing number and size of detrital geochronology data sets offer new opportunities for increased accuracy and resolution of sediment routing models. However, the new opportunities come coupled with challenges in large data integration and visualization. We address these challenges by outlining two novel approaches that aid in analyzing and interpreting large detrital geochronology data sets: (1) combination of bottom-up and top-down detrital zircon source modeling, and (2) sediment provenance mapping. Combining source-modeling methods provides guidance in identifying empirical detrital zircon sources and determining source proportions. Provenance mapping integrates source proportions from modeling results and complementary geologic data (e.g., paleocurrents, paleogeography, and stratal thickness maps) to extrapolate provenance information through areas with sparse or ambiguous data, thus mitigating issues of data distribution heterogeneity. Sediment provenance maps also provide a synoptic view of data that, along with detrital zircon source modeling, aids in circumventing lengthy descriptions of individual age modes for data sets containing hundreds of samples, which can obscure underlying trends in the data.

We apply this approach to late Paleozoic–early Mesozoic strata, using 329 published

and new U-Pb detrital zircon samples, and document five sediment-routing episodes in the core zone of intraplate deformation in western Laurentia (i.e., the Ancestral Rocky Mountains (ARM)). The transitions between these episodes are defined by changes in sediment source distribution, which are illustrated by provenance maps that show (1) the degree and extent of ARM basin isolation from transcontinental sediment sources and (2) ARM-driven changes in transcontinental sediment routing systems. We map possible sediment pathways of distally derived sediment around the ARM core, illustrating that ARM uplifts diverted transcontinental systems around areas of intense intraplate deformation. Further, the evolution of sediment routing in western Laurentia before, during, and after ARM deformation provides an example of the interaction between transcontinental sediment routing and intraplate deformation.

## INTRODUCTION

The exponential expansion of detrital zircon U-Pb data sets (Gehrels, 2014; Sundell et al., 2020) have spurred a revolution in sediment provenance analysis by creating new opportunities and challenges in data synthesis and integration (e.g., Pullen et al., 2014; Sharman and Johnstone, 2017; Chapman and Laskowski, 2019; Leary et al., 2020; Sundell et al., 2020). World-wide databases of detrital zircon ages (Puetz and Condie, 2019) enable comparison of measured samples to potential sources across the globe. However, this raises the challenge of identifying the most likely sources among an ever-expanding set of potential sources (e.g., Hervé et al., 2003; Morón et al., 2019; Clark et al., 2020; Lawton et al., 2021) particularly

during periods of supercontinent assembly. The common prospect of multiple potential sediment sources containing the same age modes presents the challenge of quantifying the contributions from those sources particularly when using individual age groups to infer source contribution. Finally, the increasing number of detrital zircon samples requires integrating information about age distribution, source identification, and source contributions in a spatial context along with complimentary geological data. In consideration of these challenges, this contribution develops new data handling and interrogation methods to better synthesize, integrate, and interpret these data.

We present a novel, integrative method of visualizing the modeled data, in concert with other geological data, to reconstruct Carboniferous–Triassic changes in sediment routing patterns in the Laurentian interior. Our approach here employs two different methods of mixture modeling to (1) develop models of sediment sources' age distributions, (2) identify the sources that best match those models, and (3) determine the proportion of detrital zircons from each source. We then contour the proportions with the aid of contextual geologic data, creating sediment provenance maps to identify the changes in sediment routing in and around the Ancestral Rocky Mountains (ARM). The utility of this approach lies in the leveraging of large data sets to analyze and interpret age distributions rather than solely focusing on individual age groups, and visualization of those data integrated with other contextual information (e.g., paleocurrent data, stratal thickness, etc.).

The upper Paleozoic–lower Mesozoic stratigraphic record in western Laurentia, which embodies all the challenges described above, is an apt interval to evaluate our modeling and visualization approach. It illustrates the

Tyson M. Smith  <https://orcid.org/0000-0003-2834-3526>

<sup>†</sup>Present address: Geosciences and Environmental Science Center, U.S. Geologic Survey, Denver Federal Center, Denver, Colorado 80225; [tysn.smith@gmail.com](mailto:tysn.smith@gmail.com).

<sup>§</sup>Present address: Department of Geosciences, Idaho State University, Pocatello, Idaho 83209, USA.

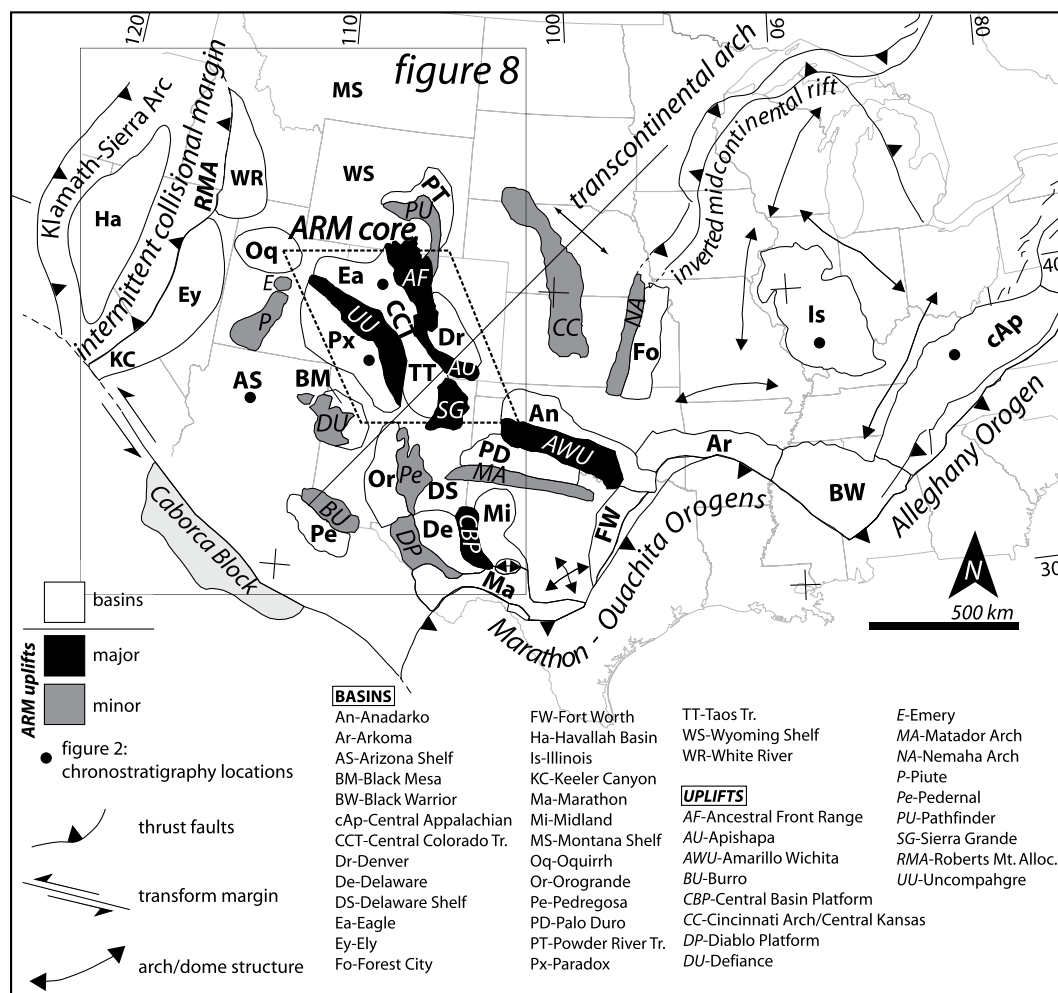


**Figure 1.** Late Paleozoic Laurentian tectonic elements including principal uplifts and basins. Map elements adapted from Kluth and Coney, 1981; Thomas, 1999; Barbeau et al., 2003; Leary et al., 2017; Lawton et al., 2017; Craddock et al., 2017; Sturmer et al., 2018. ARM—Ancestral Rocky Mountains; Tr.—Trough; Mt. Alloc.—Mountain Allochthon.

interaction between continent-scale sediment routing systems and areas of exclusive local sourcing driven by intraplate deformation. Intraplate deformation during the late Paleozoic covered a broad region of western Laurentia (a.k.a. the ARM; Fig. 1), isolating some ARM basins from distally derived sediment, and creating potential impediments to transcontinental sediment transport (Leary et al., 2020; Lawton et al., 2021). Nevertheless, Appalachian detritus derived from the eastern margin of Laurentia persisted in basins to the west of the ARM during and after ARM deformation (Dickinson and Gehrels, 2008). This apparent persistence, in part, may be due to rerouting of sediment pathways around the growing ARM. Alternatively, although not mutually exclusive, Appalachian-like detrital zircon age distributions may persist through local recycling of older strata with that signature, even if direct connection to the Appalachian orogen had been cut off. These scenarios can be discriminated by documenting sediment routing corridors before, during, and after ARM deformation and basin isolation. To do so, we

endeavor to better visualize and understand the pre-, syn-, and post-ARM tectonically induced isolation and characterize distal sediment pathways through large data set sediment source modeling and mapping of western Laurentia. Other basins where an interplay between locally and distally derived sediment occurs in time (e.g., the Amadeus Basin, Australia; Maidment et al., 2007) or space (e.g., Andean foreland of Argentina; Capaldi et al., 2017) will serve as testing grounds for the efficacy of this approach.

## GEOLOGIC BACKGROUND

The late Paleozoic (Late Mississippian–Permian) saw the amalgamation of the most recent supercontinent, Pangea. During this period Laurentia was marked by tectonic activity along its eastern, southern, and western margins (modern geographic reference frame), as well as basement-involved deformation within (Fig. 1). Along the eastern margin, the Alleghenian Orogeny (Pennsylvanian–Permian) resulted from full continent-continent collision

(Hatcher, 2010) creating a Himalayan-style mountain belt. The Ouachita-Marathon orogen resulted from a series of crustal blocks that collided at different angles and varying degrees of intensity with the uneven southern margin of Laurentia to form a mountain belt that stretched from modern-day Arkansas to west Texas, USA (Royden, 1993; Keller and Hatcher, 1999). The western and southwestern Laurentian margins underwent a complex combination of collision, back arc spreading, and sinistral translation, which has been further obscured by subsequent Mesozoic and Cenozoic tectonic activity (Trexler et al., 2004; Lawton et al., 2017; Sturmer et al., 2018).

Collision along the continental margins in the Pennsylvanian–early Permian was accompanied by the uplift of a series of basement-cored blocks and development of adjacent basins (i.e., the ARM) that stretched between present-day Oklahoma and Utah, USA (Fig. 1) (Kluth and Coney, 1981; Dickinson and Lawton, 2003; Soreghan et al., 2012; Blakey, 2019; Miall, 2019). This swath of predominantly

## METHODS

## Zircon Samples and Analytical Methods

We contribute 20 U-Pb detrital zircon samples to the existing body of published ages. New samples were collected to fill out a paucity of data within the core basins of the ARM, which include the Paradox and Eagle basins, and the Central Colorado and Taos troughs. Descriptions of samples, U-Pb age data for new samples, and ages and uncertainties for compiled data are provided in the supplemental data files (Supplemental Materials 1, 3, and 4)<sup>1</sup>.

New samples presented here were prepared at the University of Houston, Texas. Rock samples (~2 kg) were crushed and disc milled down to 400  $\mu\text{m}$  disc spacing. Mineral separation was performed using standard separation techniques: density separation via a water table followed by immersion in methylene iodide (3.28  $\text{g}/\text{cm}^3$ ), and magnetic separation on a Frantz Magnetic Separator. We used an Olympus SZX12 microscope to separate zircons from non-zircon grains after rinsing grains in nitric acid. Zircons were then non-discriminately mounted on double-sided tape.

U-Pb age of zircons were determined via ablation by Photon Machine *Excite* 193 nm ArF laser systems coupled to a Varian 810 quadrupole inductively coupled plasma-mass spectrometer (ICP-MS) at the University of Houston (Shaulis et al., 2010). Individual zircon grains were lased with 240–200 shots at 10 Hz repetition rate and 30–25  $\mu\text{m}$  spot size. We corrected for inter- and intra-element fractionation using the Bohemian Massif potassic granulite Plešovice (337.13  $\pm$  0.37 (2 $\sigma$ , two standard deviations) Ma) (Sláma et al., 2008) as the primary zircon standard. The accuracy of the fractionation correction was verified by evaluation of FC5z from

<sup>1</sup>Supplemental Material. Supplemental Material 1: Alternate source map, outliers, sample descriptions, and appendices references. Supplemental Material 2: New and previously published detrital zircon metadata table. Supplemental Material 3: New detrital zircon U-Pb reduction data. Supplemental Material 4: Detrital zircon DZnmf run table. Supplemental Material 5: DZnmf 30 source runs export for samples and sample groups (i.e., N = 191 results). Supplemental Material 6: DZmix and DZnmf results summary for 11 sources used in paper, and 11 sources plus 1.085 Ga source sample (12 sources). Supplemental Material 7: Paleocurrent metadata table. Supplemental Material 8: DZnmf 30 source runs export for individual samples (i.e., N = 329 results). Supplemental Material 9: DZmix Matlab code that allows for multiple samples to be loaded at one time and run. Please visit <https://doi.org/10.1130/GSAB.S.21554754> to access the supplemental material, and contact editing@geosociety.org with any questions.

contractional deformation initiated primarily in the Early Pennsylvanian (Leary et al., 2017; Sweet et al., 2021), occurred in Proterozoic crust (Karlstrom and Humphreys, 1998; Leary et al., 2020), and reactivated many pre-existing Proterozoic and Cambrian rift structures (Marshak et al., 2000; Craddock et al., 2017). ARM uplifts were thrust onto adjacent crust (Frahme and Vaughn, 1983; Brewer et al., 1983; Hoy and Ridgeway, 2002) creating flexural basins that accommodated detritus shed from the bounding uplifts (Barbeau, 2003; Soreghan et al., 2012). The core of the ARM straddled the trace of the transcontinental arch (Carlson, 1999; Leary et al., 2020), which was a continental-scale, long-lived, northeast-southwest trending feature (Fig. 1) that controlled deposition in the midcontinent and western Laurentia throughout the early–middle Paleozoic (Sloss, 1988; Linde et al., 2014; Linde et al., 2017).

Upper Mississippian fluvial rocks of the Grand Canyon area (a.k.a. the Arizona shelf) record the arrival of a characteristic detrital zircon age distribution interpreted to mark the sediment routing connection between the Appalachian Mountains and the western shores of Laurentia (Gehrels et al., 2011; Gehrels and Pecha, 2014; Attia et al., 2018; Chapman and Laskowski, 2019). This age distribution is defined by a positively skewed “Grenville” mode (0.95–1.3 Ga, peak at ca. 1.1 Ga), and subordinate Paleozoic–late Neoproterozoic modes (Gehrels et al., 2011; Chapman and Laskowski, 2019; Kuiper and Hepburn, 2020). The arrival and subsequent persistence of these age modes suggest that during the rest of the Paleozoic, a relatively continuous supply of eastern-derived sediment was routed to the western Laurentian margin. Prior to the introduction of this eastern-sourced age distribution, detrital zircon ages in older units were predominantly late Paleoproterozoic and early Mesoproterozoic (Fig. 2), reflecting first-cycle or recycled western Laurentian crustal detritus (Gehrels et al., 2011; Chapman and Laskowski, 2019). Appalachian or Appalachian-like detrital zircon age distributions, potentially contributed by other sources (e.g., Ouachita-Marathon sourced sediment), persisted in the successive sedimentary record of western Laurentia throughout the late Paleozoic–early Mesozoic and beyond (Dickinson and Gehrels, 2008; Gehrels et al., 2011; Liu and Stockli, 2019; Gao et al., 2020; Thomas et al., 2019).

Research indicates that the transcontinental sediment transport system began to grow from east to west across Laurentia in the Mississippian and was aided by shallow marine processes (e.g., tides, longshore currents, storms; Chapman and Laskowski, 2019). Other potential sediment sources from along the Laurentian margin bear-

ing varying degrees of similarity to the Appalachian detrital zircon age distribution include the Ouachita-Marathon front (Thomas et al., 2019), the Arctic Ellesemerian mountains (Beranek et al., 2010; Anfinson et al., 2012; Leary et al., 2020), and the remnant Antler uplifts in Idaho and Nevada, USA (Linde et al., 2016; Beranek et al., 2016). Despite the influx and mixing of sediment from around Laurentia, many ARM basins, especially in the core of the ARM (Fig. 1), contain large regions of dominantly locally derived sediment (Leary et al., 2020). The temporal overlap of areas dominated by local versus distal provenance raises questions of what controlled the geographic distribution of sediment source through time. Further, what was the extent of ARM basin sediment source isolation and how were distally derived sediments delivered to the western margin of Laurentia during this time?

ARM deformation ceased in the early Permian, but post-tectonic infilling of some ARM basins continued into the middle and late Permian (Dickinson and Lawton, 2003), and remnant uplifts affected sediment routing through this area into the Mesozoic (Dickinson et al., 2010). By Permian time, increased aridity resulted in pervasive eolian sediment transport across western Laurentia (Leary et al., 2020; Lawton et al., 2021), and during the late Permian, much of this region experienced nondeposition and/or erosion (McKee and Oriol, 1967). Relatively brief Early–Middle Triassic deposition in marine and nonmarine settings (e.g., Moenkopi Formation) occurred in the flexural basin of the Sonoma Orogen along western Laurentia (Lawton, 1994; Dickinson and Gehrels, 2008), and was followed by another period of nondeposition and/or erosion. Arc collision along Laurentia’s western margin in the Late Triassic created back-arc rift-related accommodation, preserved transcontinental fluvial deposits, and set the tectono-stratigraphic stage for the remainder of the Mesozoic (Dickinson and Gehrels, 2008; Dickinson, 2018). Plutonic rocks exposed in southern California (USA) record development of the southern magmatic arc from late Permian to Late Triassic along the truncated southwest margin of Laurentia (Riggs et al., 2013; Cecil et al., 2018). In the Late Triassic, arc material from this southern margin was transported northeast into a northwest-directed fluvial system (Dickinson and Gehrels, 2008; Riggs et al., 2016). The headwaters of this northwest-flowing fluvial trunk resided in the remnant Ouachita-Marathon mountains and their exhumed foreland basins, which delivered sediment from south Texas to western Arizona and Utah (Dickinson and Gehrels, 2008; Dickinson, 2018).



**Figure 2. Chronostratigraphy of selected North American (N.A.) depocenters from Late Devonian through Triassic showing the relative contribution of local source (red) versus distal source (blue) zircon contributions based on coupled bottom-up and top-down mixture models. Purple area within the distal source swatch indicates the Triassic arc component. Figure also contains detrital zircon age spectra (kernel density estimate (KDE), 20 m.y. bandwidth) for modeled samples and timing of N.A. tectonic episodes. R<sup>2</sup>s (coefficients of determination or cross-correlation coefficients) from top-down model matches are displayed to the upper left of associated KDEs and n-values are displayed to the upper right. ARM sedimentation episodes are displayed on the right side. Note that the samples shown here are only a portion of the published and new samples used in this study. Timescales adapted from Aretz et al. (2020), Henderson and Shen (2020), and Ogg and Chen (2020). (B) Laurentian tectonics: Dickinson and Lawton (2003), Trexler et al. (2004), Dickinson (2018). (Ci) Arizona shelf stratigraphy: Gehrels et al. (2011), Lawton et al. (2015), Dubiel and Hasiotis (2011), Blakey (2008); detrital zircon samples and sample groups: Temple Butte group (SG), Surprise Canyon SG., Watahomigi, Manakacha, 06GC147, Esplanade SG., Hermit SG., Coconino SG., Toroweap SG., Kaibab SG., and Chinle 2SG. (Cii) Paradox Basin stratigraphy: Condon (1995), Gianniny and Miskell-Gerhardt (2009), Lawton et al. (2015), Blakey (2008), Barbeau (2003); detrital zircon samples and sample groups: SJMT1, Molas SG., MP-DZ2, combination of SJMT3 and SP01, SJMT4, Cutler 3 SG., White Rim SG., CP47, CP50. (Ciii) Eagle Basin: Condon (1995), Webster and Houck (1998), Johnson (1987), Blakey (2008), Soreghan et al., 2014; Irmis et al. (2015); detrital zircon samples and sample groups: Leadville SG., CC01, Eagle Valley 1 SG., Minturn SG. 1, Maroon 1 SG., 2RFMMT383, and CP4. (Civ) Illinois Basin stratigraphy: Shaver et al. (1986), Kolata (2005), Kissock et al. (2018); detrital zircon samples and sample groups: IB-D4, IB-D3, Tradewater-Shelburne-Carbon SG., Caseyville-Tradewater SG., 14M03, and 14M04. (Cv) Appalachian Basin stratigraphy: Kreisa and Bambach (1973), Donaldson et al. (1985), Martin (1998), Eble et al. (2009), Chestnut and Greb (2009); detrital zircon samples and sample groups: Washington-Greene SG., Pottsville-Sharon SG., and Princ-Bluest-Hint SG. For detrital zircon sample and sample group references see Supplemental Material 2. *DZmix*—top-down detrital zircon source modeling code (Sundell and Saylor, 2017); n—number of analyzed grains; N—number of samples; Ls.—limestone; ARM—Ancestral Rocky Mountains; undiff.—undifferentiated; Dev.—Devonian; Geologic ages: Rhaet.—Rhaetian; Ladin.—Ladinian; Anisian.—Anisian; Olenek.—Olenekian; Ch.—Changhsingian; Wuc.—Wuchiapingian; Road.—Roadian; Wor.—Wordian; Capt.—Capitanian; Sak.—Sakmarian; Kungar.—Kungarian; Bashkir.—Bashkirian; Moscov.—Moscovian; Kas.—Kasimovian; Gzh.—Gzhelian; Mor.—Morrowan; Desm.—Desmoinesian; Mi.—Missourian; Virg.—Virgilian; Serpukh.—Serpukhovian; Kinder.—Kinderhookian; Famen.—Famennian.**

the Duluth Complex ( $1099.1 \pm 0.5$  ( $2\sigma$ ) Ma) (Paces and Miller, 1993) as the secondary standard. Analyses of every 10 unknowns were separated by an analysis of the primary standard. In turn, every third analysis of the primary standard was coupled with a secondary standard analysis.

Ages were determined with U-Pb Toolbox, a MATLAB-based application, which calculates integrated isotopic ratios from raw counts per second that are exported from Quantum software, corrects for machine bias and fractionation, and filters the databased on user-defined parameters (Sundell, 2017). Zircons were filtered using a 15% uncertainty cutoff, and 20% and  $-10\%$  discordance cutoffs ( $^{206}\text{Pb}/^{238}\text{U}$ – $^{207}\text{Pb}/^{235}\text{U}$  ratio, the latter determined via measured  $^{207}\text{Pb}/^{206}\text{Pb}$  and the accepted  $^{238}\text{U}/^{235}\text{U}$ , 137.82) applied with a 900 Ma discordance transition. Instead of a common Pb correction (Stacey and Kramers, 1975), we accept grains whose  $2\sigma$  envelope is  $<15\%$  discordant by comparison of the  $^{206}\text{Pb}/^{238}\text{U}$  and  $^{207}\text{Pb}/^{235}\text{U}$  ages for ages  $<600$  Ma.

### Sediment Source Modeling

Sediment source modeling and comparative statistical metrics provide quantitative tools to distinguish distinct source signals and identify similarities amongst age distributions in the ever-increasing volume of provenance data (Amidon et al., 2005; Vermeesch, 2012, 2013; Saylor and Sundell, 2016; Sharman and Johnstone, 2017). The approach adopted here merges the strengths of bottom-up and top-down model-

ing (Fig. 3) to avoid lengthy and often cumbersome descriptions of individual age modes for large data sets. It does so by characterizing possible source distributions, and the proportions of sources assigned to individual samples. Both bottom-up and top-down models include goodness of fit metrics that assess how well generated model distributions match the sample distributions that they are trying to recreate. Top-down and bottom-up sediment unmixing models are defined by whether known sources are used as an input, and how the algorithm determines source attribution to sink samples (i.e., samples from basin(s), which are being analyzed) (Sharman and Johnstone, 2017).

How do we determine what the actual detrital zircon sources looked like, especially in ancient basins? Bottom-up modeling answers this question and does so with no known source input. Rather, this method aims to determine unknown sources that contributed to the collection of sink data distributions (Sharman and Johnstone, 2017). Bottom-up modeling used here employs a non-negative matrix factorization (NMF) algorithm to deconvolve two matrices that define (1) a series of synthetic sources (a.k.a. factorized sources) and (2) corresponding weighting functions both from an input matrix composed of sample's age distributions from a basin or basins (i.e., sink data set) (Sharman and Johnstone, 2017; Saylor et al., 2019). The deconvolved matrices are iteratively updated with the goal to minimize the error (e.g., final residual) between model and sample age distributions for

a given number of factorized sources (Saylor et al., 2019). To identify the optimal number of factorized sources, we considered three ranks (i.e., factorized source sets) centered on the rank above which there is little or no decrease in the final residual (Fig. 4A) (Saylor et al., 2019). To discriminate among these three factorized source sets, we use geologic information (e.g., knowledge of realistic sediment sources within the study area, previously proposed sediment sources) to determine which set of factorized sources most accurately depicts the dominant detrital zircon sources in the study area. Thereby using the bottom-up approach to identify the empirical detrital zircon sources to be selected for top-down mixing.

Top-down models mix proportions of detrital zircon sources from sample data (i.e., empirical sources) to create a mixture distribution that most closely matches that of a given sink sample (e.g., Amidon et al., 2005; Saylor et al., 2013; Kimbrough et al., 2015; Licht et al., 2016; Mason et al., 2017). Here, we mix empirical source age distributions via the Monte Carlo approach of *DZmix* (Sundell and Saylor, 2017) to create a model age distribution from a random mixture of these inputs, and then compare that modeled distribution to a detrital zircon sample age distribution from our sink data set. This process is repeated many times (e.g., 10,000) for each sample in the sink data set, and the best matches are retained. If the input sources closely reflect the actual detrital sources, then the proportions of input sources assigned to the best fit

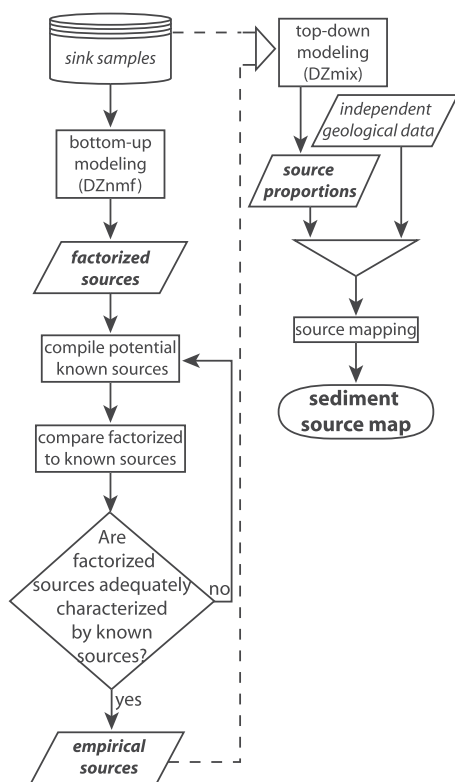


**Figure 3.** Flow chart that schematically describes the approach of source characterization and source visualization described in this paper. Data inputs are italicized, and products are in bold. Objects that are both bold and italicized are products that also serve as inputs. **DZmix**—top-down detrital zircon source modeling code (Sundell and Saylor, 2017); **DZnmf**—bottom-up detrital zircon source modeling code (Saylor et al., 2019).

models for each detrital zircon sample faithfully approximate actual detrital source proportions.

### Source Modeling Algorithm

#### Step 1: Bottom-Up Sediment Source Modeling

In the first step, we used **DZnmf** (Saylor et al., 2019) to deconvolve (a.k.a. factorize) a set of 191 Devonian–Triassic Laurentian detrital zircon samples and sample groups (i.e., model inputs) into a set of potential detrital zircon sources. We use the optimal number of sources suggested by the **DZnmf** (Fig. 4A) to guide our selection of source sets within the context of our geologic understanding of sediment routing in western Laurentia during this time (the process described below). The data used in modeling span North America and were distilled from 329 individual samples by grouping geologically and geographically adjacent samples. This curation of the data better characterizes age distri-

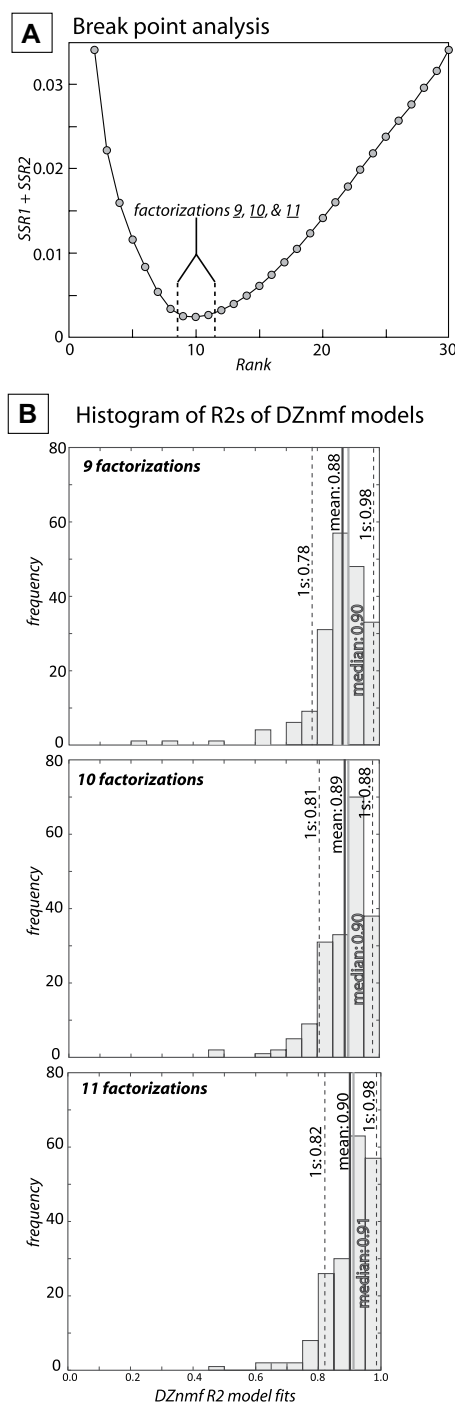
**Figure 4.** **DZnmf**—bottom-up detrital zircon source modeling code (Saylor et al., 2019)—break point analysis (A) and factorizations for sources 9–11 (B). (A) Factorized sources 9–11 are bracketed to illustrate the synthetic source sets that we evaluated to determine the preferred number of sources to use in subsequent steps of empirical source identification. Rank, along the x-axis, is the number of synthetic sources produced by **DZnmf** for each factorization. SSR is the summed square residual, and SSR1 and SSR2 are the expected residuals for the lower and higher rank line segments, respectively, calculated via linear regression (Saylor et al., 2019). (B) Histogram plots of  $R^2$  values for **DZnmf** model fits for factorization runs using synthetic sources 9, 10, and 11.

butions by combining samples, which thereby increases sample size ( $n$ ). To address the potential mismatched lumping of samples into sample groups, we also performed this exercise without any lumping (i.e., running 329 individual samples through **DZnmf**; see Supplemental Material 8 for results). Minor differences are noted in the results below, but none that we found to affect the overall results or interpretations of this study, especially with respect to empirical source identification. All calculations in the following sections are based on kernel density estimates (KDEs) with a 20 m.y. bandwidth. We use KDEs rather than PDPs, which use analytical uncertainty for bandwidth, to mitigate mismatches of analytical precision associated with the range of analysis types (e.g., laser ablation ICP-MS versus secondary ion mass spectrometry) (Vermeesch, 2012).

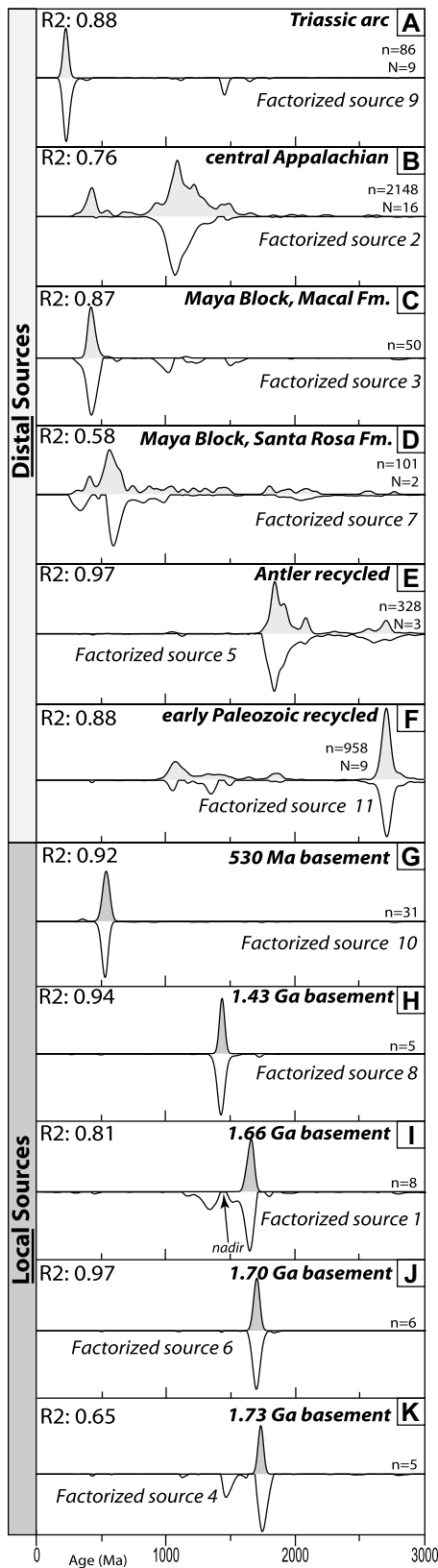
#### Step 2: Identification of Empirical Sources

In the second step, we search for and identify empirical sources that match the factorized sources produced in Step 1 with **DZnmf**. Empirical source matches were selected based on their similarity to factorized age distributions (Fig. 5; Table 1). Here, we used coefficient of determination ( $R^2$ ) from cross-correlation to determine best empirical source match. The searching and identification of potential sources is often iterative (Fig. 3) because initial sources identified may yield low similarity, sending the researcher back into the literature to find a better match. We discuss the uncertainty and relevance of our detrital zircon source selection in the context of possible late Paleozoic and Triassic sediment sources.

We interpret some of the empirical sources to directly reflect the location of detrital zircon sources. However, other factorized sources are



non-unique, and share similarities to multiple empirical sources. Nevertheless, even in these cases, a broad distinction can be drawn between sediment derived from basement sources adjacent to the ARM basins and sediment transported from terranes on the margins of Laurentia. This level of detail works well for the types of sediment sources that existed during the study interval, and discrimination of ARM-driven sediment routing and basin isolation. In cases of applying this approach where a broad



distinction is not sufficient in addressing provenance questions, further data would need to be brought to bear.

**Figure 5. Factorized (white fill) source to kernel density estimate (20 m.y. bandwidth) (color fill) comparison with respective cross-correlation coefficients. See Table 1 for empirical source details. n—number of analyses; N—number of samples; Fm.—Formation.**

**Step 3: Top-Down Sediment Source Modeling**

In the third step, we complete the sediment source modeling loop by top-down modeling the sink sample data set that was used in bottom-up modeling (i.e., Step 1). Top-down modeling also uses the empirical source set developed in Step 2. Utilizing both of these data sets, we model the proportions of empirical sources for each sink sample via the MATLAB-based DZmix algorithm (Sundell and Saylor, 2017). However, we employ an edited version of this code that allow analysis of all the detrital zircon samples at once, and which is included in Supplemental Material 9.

Parameters for the model were set at 10,000 runs and we retained the best 0.1% fits to create mean model distributions. We compare bottom-up and top-down model results to assess consistency across model predictions (Fig. 6; Supplemental Material 1). DZmix produces best model fits for R<sup>2</sup>, Kuiper V statistic, and Kolmogorov-Smirnov D statistic. We use the R<sup>2</sup> model results and compare these results to Kuiper V statistic to check consistency. When interpreting model results, we focus on the major contributors to age distributions, and discount sources whose contributions are within uncertainty of zero.

**Step 4: Sediment Source Mapping**

Visualization of provenance evolution in both time and space is a powerful approach to understanding and interpreting source-to-sink data. In this study, sediment sources are broadly defined by the zircon age distributions that they contribute. This research focuses on the degree of ARM-driven provenance isolation within a background of continental-scale sediment mixing. We use the character of U-Pb zircon age distributions found in the stratigraphic record to discern these local and distal sediment source signals. Therefore, sediment sources identified in bottom-up modeling, and prescribed in top-down modeling are lumped into two categories: (1) Local contributors of sediment, which constitute many of the basement-cored ARM uplifts, and (2) contributors of sediment distal from the core of the ARM, which tend to reside along the Laurentian margin (Figs. 5 and 7). The recipients of sediments from these two sources (i.e., detrital zircon samples) are visualized primarily based on the percentage of source attribution. This approach to grouping samples is designed to fit

our focus of ARM-driven provenance isolation, and is not inherent to the data or the approach. This focus also guides the types of auxiliary data used to aid in contouring provenance maps.

Local sources, as defined here, contribute sediments that are characterized by unimodal age distributions that reflect Laurentian basement exposed in ARM uplifts, or recycled from similarly sourced lower Paleozoic strata (Fig. 7). On occasion, further distinction in the local source attribution is made by considering the composition of the sandstone, and where available, published descriptions of sandstone compositions are used to interpret direct from basement versus recycled sediment source (e.g., arkosic versus quartz-rich). The distal sediment source group is predominantly attributed to empirical source matches from the Laurentian margin and associated accreted terranes (Fig. 7). Most of these sediment source signals are characterized by multi-modal age distributions, and although some exhibit simple age distributions, they are not commonly associated with basement exhumed by ARM deformation (e.g., Archean; Leary et al., 2020). This binary categorization is intended to collapse some of the ambiguity in identifying specific sediment sources. Whereas most sediment sources can be confidently attributed to either local basement or distal margin, the specific location of sources for some samples may remain somewhat ambiguous.

Sediment source proportions from DZmix results (Supplemental Material 6) were contoured with the aid of stratigraphic thickness maps, paleocurrent data, and paleogeographic information (Supplemental Material 1) to create sediment source maps (Fig. 8). Paleocurrent data (Supplemental Material 7) were used to help infer direction of sediment routing. These data are plotted on provenance maps and colored based on the general mechanism of sediment transport (i.e., eolian versus fluvial/alluvial or deltaic/marine). We contributed 18 paleocurrent measurement stations to 201 published paleocurrents. New paleocurrent stations each contain 5–25 individual measurements (n = 288), and are comprised of trough crossbedding, planar crossbedding, and imbricated clast measurements.

We use a large contour interval (20%), which is intended to compensate for the degree of variability within the sediment source episode and the uncertainty of top-down model results. The few instances where closely spaced samples exhibit variability greater than the contour interval commonly reflect temporal changes in sourcing that are beyond the resolution of the selected time interval (i.e., sediment source episode, which is defined below). For example, in Atokan-Wolfcampian Episode 3, one of the several samples in the middle Paradox Basin yields a 73% local

TABLE 1. TABLE CONTAINS COMPARISONS BETWEEN EMPIRICAL (I.E., GEOLOGIC) AND FACTORIZED SOURCES AND METADATA FOR EMPIRICAL SOURCES

Empirical source match	N	n	Factorized source	R <sup>2</sup>	Reference	Sample(s)
Triassic arc	9	86	9	0.88	Riggs et al. (2016)	110609-1C, 110609-1E, JC-7, JCNEW-2D, 120309-1F, 120309-1H, 050511-2C, 103009-1C, 103009-1H
Central Appalachian	16	2148	2	0.76	Thomas et al. (2004); Becker et al. (2005); Becker et al. (2006); Park et al. (2010); Thomas et al. (2017) Thomas et al. (2019)	Princeton, Bluestone, Hinton, Mauch_Chunk, KY-21-SG, Tumbling Run, Pottsville Fm., Pocohontas, Lee, Racoon, Montevallo, Sewanee, KY-18-CB, VA-1-GN, OH-4-SN, OH-1-SS
Coahuila terrane	12	902	2	<i>0.68, 0.64, 0.23</i>		*08NR02, 08NR03, PC01, PC02, PC03, PC04, LR1, TCP2, SM2, PAT1, COALC4, COALC5 (removed grains <340 Ma, < 300 Ma, < 250 Ma)
Sabine terrane	5	286	2	0.58	Shaulis et al. (2012)	*2011-1, 2010-1, 2010-2, 2010-5, 2010-6 (removed grains <340 Ma)
Maya Block, Macal Fm.	1	50	3	0.87	Martens et al. (2010)	BZ05
Maya Block, Santa Fe Fm.	2	101	7	0.58	Weber et al. (2006)	CB55, SR01
Northern Appalachian	2	521	7	0.43	Kissock et al. (2018)	FCB-D4, IB-D1
Antler recycled	3	328	5	0.97	Beranek et al. (2016)	06PL13, 09TD10, 02TD10, 24PL09, 05PL15, 09LB04
Early Paleozoic recycled	9	958	11	0.88	Pickell (2012)	BC, CR, USSB, BM, TM, BT, TCT, S5, AS2
530 Ma	1	31	10	0.92	Smith et al. (2023)	SAFT8
1.43 Ga	3	3	8	0.94	Bickford et al. (2015)	KSMS-044, KSMS-046, KSMS-047
1.66 Ga	1	8	1	0.81	Amato and Becker (2012)	06KD-02
1.70 Ga	1	6	6	0.97	Guitreau et al. (2016)	Cgg-8
1.73 Ga	1	5	4	0.65	Jessup et al. (2006)	J01-BC5

*Notes:* Empirical sources not used in the top-down mixture modeling source profile are designated with italicized coefficient of determination ( $R^2$ ) and factorized source number. Descriptions of  $R^2$  in the text reflect the following groups: very high ( $R^2$ : 1.0–0.9), high ( $R^2$ : 0.9–0.7), moderate ( $R^2$ : 0.7–0.5), poor ( $R^2$ : 0.5–0.3), and very poor ( $R^2$ : >0.3) correlation. Coahuila terrane source is amalgamated from Mesozoic rocks presented in Thomas et al. (2019). Because these rocks post-date the study interval (i.e., late Paleozoic–Triassic), we removed grains with younger ages.  $R^2$ s presented correspond to the amalgamated samples being truncated at 340 Ma, 300 Ma, and 250 Ma, as described above in the sample(s) column. Sabine terrane source consists of several tuff samples from the Stanley Group (Shaulis et al., 2012) from which we removed grains <340 Ma to isolate potential Sabine terrane crustal zircons (Thomas et al., 2021). Fm.—Formation.

\*Indicates that grains from samples we removed to eliminate erroneous or confounding data.

(i.e., basement or recycled basement) source contribution, and is surrounded by samples with  $\geq 80\%$  local contribution (Fig. 8C). We italicize this value in the source map to indicate the discrepancy and contour with consideration of all data points in the area (i.e., place the 80% local sediment source contour adjacent this point in the data cluster). In an absolute sense, this difference is not significant. However, it is important to understand why these discrepancies exist. We divide the study interval (Carboniferous–Triassic) into five episodes (Fig. 2A) and create sediment provenance maps for each, the details of which are covered in the Discussion section of this paper. The boundaries between episodes, defined here by trends observed in the provenance record, coincide with North American stages. However, the sedimentation regimes that define these episodes reflect tectono-sedimentary processes that do not necessarily turn off and on at stage boundaries. Therefore, episode boundaries are somewhat imprecise (Fig. 2A). Many formations from which samples were collected have age designations that span stage and episode boundaries. In these cases, where no further stratigraphic information may be brought to bear, we either assume a midpoint age or assign the sample to the episode containing other nearby samples that exhibit similar characteristics.

## RESULTS

As sample numbers increase, it is increasingly cumbersome to present, describe, and discuss age distributions for each sample. The bottom-up modeling described above addresses this and

allows us to focus on salient endmember features of the 191 samples and sample groups included in this study. Therefore, in the following section we discuss source distributions and their attribution to detrital zircon samples from basins. We also present both top-down model results and KDEs for selected detrital zircon data (Fig. 2C) to provide a basis for comparison between the more granular approach of visualizing each sample's age distribution and the higher-level data analysis of the modeling and mapping approach proposed here (Figs. 3 and 8).

### Step 1. Bottom-Up Modeling

Bottom-up modeling with DZnmf indicates an optimal number of sources is 10 (i.e., low rank minimum final residual or breakpoint; Saylor et al., 2019); however, factorization of 9 and 11 source models yield similarly low residuals and are considered here (Fig. 4A). Mean and medians of  $R^2$  values for factorization models and sample distributions do increase from 9 to 11 (Fig. 4B), but factorization 11 identifies an additional Laurentian crustal age (i.e., 1.74 Ga, see Step 2 below for further description) that we interpret to be an important component of ARM basin sediment supply. We therefore use results from the 11-source factorization, which yield generally high correlation and low residuals (i.e., the difference between mixed models and corresponding sink samples) for factorized source mixed models and sample age distributions (Fig. 4). The 11-source factorization models compared to sink sample age distributions yield mean and median  $R^2$  of  $0.90 \pm 0.08$  ( $1\sigma$ , one

standard deviation) (Fig. 4B) and 0.91, respectively, and Kuiper V statistics of  $0.07 \pm 0.04$  ( $1\sigma$ ) and 0.07, respectively.

To determine what, if any, effect our sample groupings have on the factorization of sources, we also used a bottom-up modeling approach on the 329 individual samples (Supplemental Material 8), and compared the results with the results from the bottom-up model using the 191 grouped samples (Supplemental Material 5). The most notable differences in the 329-sample model are the absence of a ca. 2.7 Ga age distribution, the presence of a 1.085 Ga unimodal source, and a corresponding 1.085 Ga nadir in an age distribution that is otherwise consistent with a “Grenville” source (Fig. 5B). The splitting of the “Grenville” age mode does not appear to lend any insight into better empirical matches. Furthermore, nadirs in age distributions that correspond to modes in other distributions are common artifacts in NMF detrital zircon modeling (Leary et al., 2020), and we therefore discount the 1.085 Ga nadir as an artifact. This reduces the differences between the models using the 329 individual samples and the 191 grouped samples from three to two: (1) elimination of the Archean source and (2) addition of the 1.085 Ga source. The Archean source is a relatively minor contributor in comparison to the other empirical sources. Its elimination would most likely force top-down models to attribute other empirical sources containing approximately similar age distributions while yielding poorer model fits (as observed in the 329 model: Supplemental Material 8). The 1.085 Ga source is indeed a minor, but unique contributor to (mostly) Pennsylvanian–Permian sink samples



used as empirical sources, which are matched to factorized sources, to be the only locations from where those sources are attributed. Rather, the empirical sources are representative of detrital zircon source regions to varying degrees of geographic specificity, which is discussed for each source below. For, example, factorized source 10 is matched to our 530 Ma basement empirical source, which is perhaps the most spatially limited source proposed here. The sample we use for that empirical source is from Cambrian igneous rocks exposed in Colorado, but is used in the proposed source set to represent detrital zircons from several Cambrian igneous rock exposures across the midcontinent and western Laurentia. Many of the factorized sources discussed here are like factorized sources presented in Leary et al. (2020), which we present a brief comparison to in the discussion below.

### Distal Sources

**Triassic arc.** Factorized source 9 exhibits a dominant unimodal age distribution at ca. 230 Ma and exhibits a high correlation ( $R^2$ : 0.88) to the zircon age distribution from volcanoclastic gravels in Triassic sedimentary rocks of southwestern North America (Riggs et al., 2016) (Fig. 5A). We interpret attribution of this source to represent volcanic material shed from the Mesozoic Cordilleran magmatic arc that stretched along the southwestern margin of Laurentia (Fig. 7) (Riggs et al., 2012). There is a minor age population at ca. 1.46 Ga in the factorized source that is not in the empirical source and therefore not incorporated into top-down models. Both top-down and bottom-up models identify this source only in Triassic basin samples.

**Central Appalachian.** Factorized source 2 exhibits a positively skewed broad age mode (a.k.a. Grenville age mode; 0.95–1.3 Ga) centered at ca. 1.1 Ga and is highly correlated ( $R^2$ : 0.76) to the central Appalachian empirical source (Fig. 5B). In most cases, we interpret attribution of this source to indicate detrital zircons originally shed from the growing Appalachian Mountain belt in the late Paleozoic. We also compared a few other possible empirical source matches to factorized source 2, but all other comparisons yielded poorer correlations (Table 1). These other samples are representative of accreted peri-Gondwanan terranes along southern Laurentia (i.e., Coahuila and Sabine terranes; Fig. 7). Despite their comparatively lower correlation to factorized source 2, we acknowledge the possibility that peri-Gondwana terranes may have contributed detrital zircons bearing a similar age distribution (Thomas et al., 2019, 2021), especially in strata deposited along the southern margin of Laurentia. Due to this source area ambiguity, we use regional

### DZmix vs. DZnmf $R^2$ s

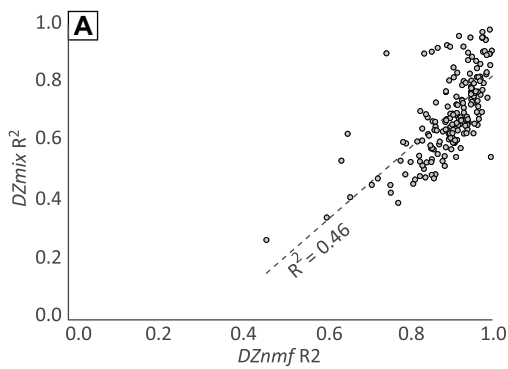
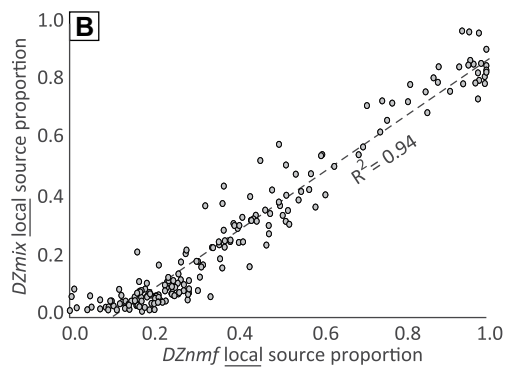
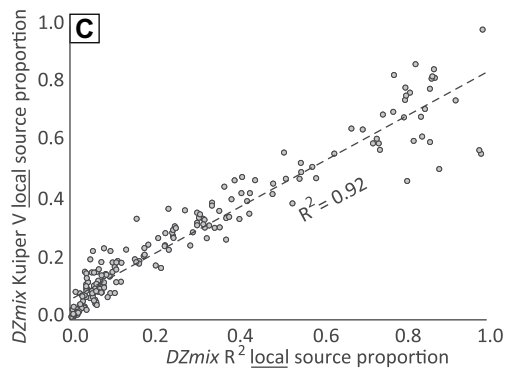


**Figure 6.** (A) Cross-plots of bottom-up (DZnmf) and top-down model (DZmix)  $R^2$ s between corresponding samples. (B) Cross-plot of local source attribution between corresponding samples in DZnmf and DZmix. (C) Cross-plot of local source attribution comparing  $R^2$  and Kuiper V DZmix models.  $R^2$  (coefficient of determination) and Kuiper V statistic are approaches to evaluate the similarity between two distributions, here applied to age distributions. The former compares the age distributions in the form of KDEs (in this application) via cross-plot (Saylor and Sundell, 2016), whereas the latter compares the cumulative density functions (CDFs) and sums the absolute values of the maximum and minimum differences (Kuiper, 1960).

### DZmix vs. DZnmf local source attribution



### DZmix models: $R^2$ vs. Kuiper V local source attribution



in western Laurentia that has a realistic empirical source match. We experimented with including this empirical source in top-down models and provenance maps, but ultimately decided against it. Details of these models are covered in the Discussion: Consideration of the Methods section as well as Supplemental Materials 1 and 6.

## Step 2. Comparison of Factorizations to Empirical Sources

We compare the 11 factorized sources from the bottom-up modeling approach to several

empirical sources with the aim to produce an empirical source set. The following sections describe and compare the factorized sources and empirical sources (Table 1; Fig. 5). Our goal is to find empirical sources that closely match factorized ones, and then to use those empirical sources in top-down modeling (i.e., Step 3). The empirical source set that we propose here and use in subsequent steps exhibits very high-moderate correlation to their factorized counterparts with a mean  $R^2$  of  $0.84 \pm 0.13$  ( $1\sigma$ ) and a median of 0.88. It is important to note that we do not intend for the exact locations of the samples

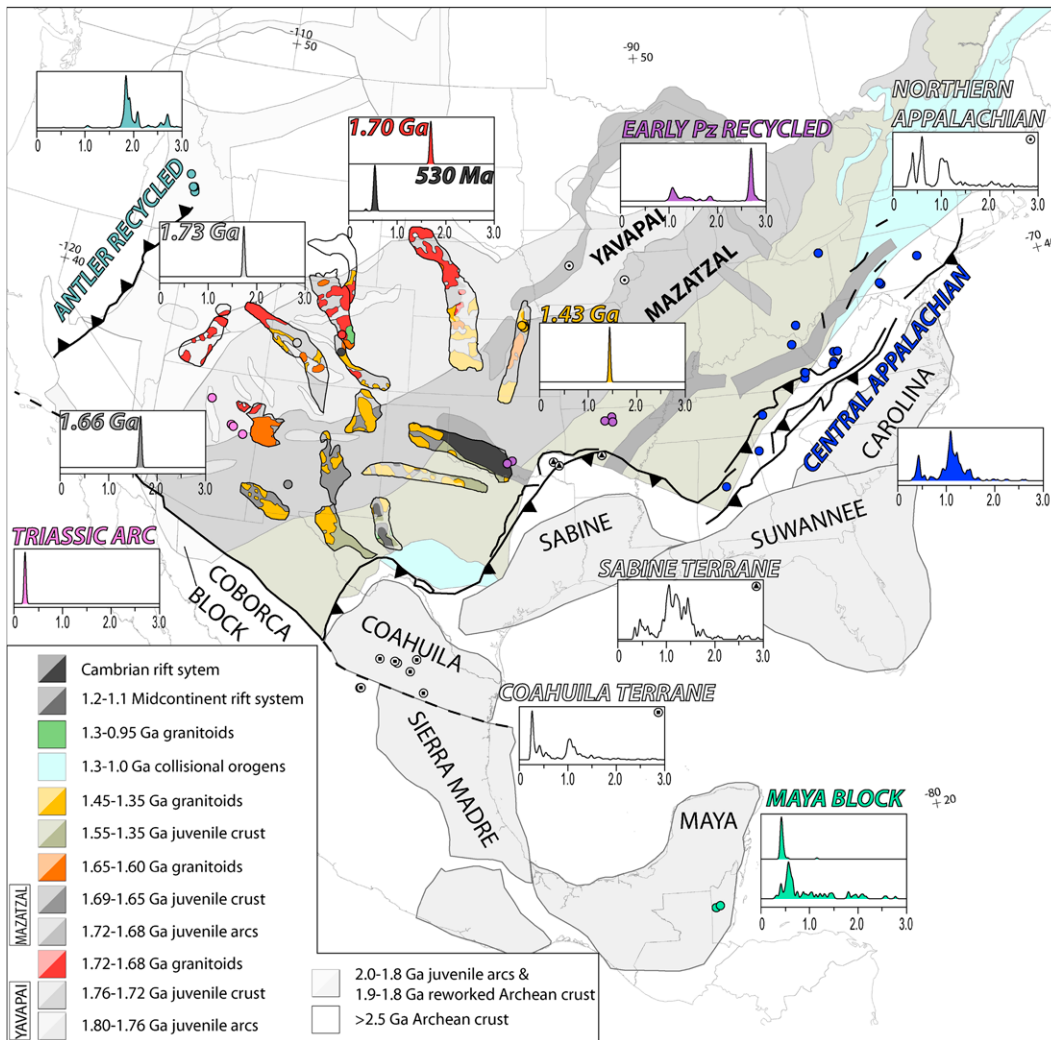


**Figure 7.** Map of late Paleozoic to Triassic sediment sources discussed in text. Data points for samples used to characterize potential sediment sources are colored the same as the corresponding kernel density estimate (20 m.y. bandwidth) in this figure and in Figure 4. Position of the Maya Block relative to Laurentia is in its present-day location; however, during the late Paleozoic, the Maya Block would have shared its northern margin with the southern margin of the Sabine terrane with the North Gondwana arc located between them (Lawton et al., 2021). See Table 1 for details on source data. Laurentian crustal terranes and granitoids are adapted from Whitmeyer and Karlstrom (2007). Granitoids are shown only in areas of Ancestral Rocky Mountain uplift. Accreted terranes of southern Laurentia and modern-day Central America are adapted from Dickinson and Lawton (2001) and Thomas et al. (2019). Areas of white transparency overlain on Laurentia indicate that basement detritus was not sourced from these areas as they were either sites of

deposition, not areas of active uplift, and/or exhibit early Paleozoic sedimentary cover beneath the base of the Pennsylvanian strata (McKee and Crosby, 1972). Pz—Paleozoic.

paleocurrent data and additional age modes to help guide our interpretation (see discussion of factorized sources 3 and 7 below).

**Maya Block.** Factorized sources 3 and 7 predominantly exhibit early Paleozoic and late Neoproterozoic age distributions, respectively (Figs. 5C and 5D). We broadly interpret factorized sources 3 and 7 as representing detrital zircons shed from terranes that collided along the southern and/or eastern Laurentian margin. We select empirical source matches that yield high ( $R^2$ : 0.87) and moderate ( $R^2$ : 0.58) correlations to the upper Paleozoic Macal and Santa Rosa formations, respectively, which are exposed in present-day Central America (Fig. 7). These strata are interpreted as a flysch sequence deposited along the northern edge of Gondwana during a complex collision between other peri-Gondwanan terranes, Gondwana, and Laurentia during the late Paleozoic (Weber et al., 2006,

2008). This empirical source match is consistent with recent provenance interpretation of similar age distributions in the Marathon and Permian basins that used both detrital zircon U-Pb and Hf isotope compositions ( $\epsilon\text{Hf}(t)$ ; Thomas et al., 2019). However, similar late Neoproterozoic and early Paleozoic detrital zircon age populations are also observed in mid-continent basins, and they are attributed to a northern Appalachian source (Kissock et al., 2018; Thomas et al., 2020; Leary et al., 2020). The primary cause of the conflicting source attribution for these detrital zircon ages is the similar Neoproterozoic–early Paleozoic geologic and magmatic histories of many peri-Gondwanan terranes (Murphy et al., 2004; Pollock et al., 2012). Despite provenance attribution ambiguity, these source ages may provide a tool in discriminating between eastern and southern Laurentian margin provenance in future research. Detailed investigation

of these late Neoproterozoic and early Paleozoic detrital zircon age populations that employ auxiliary provenance proxies (e.g., detrital zircon Hf isotope compositions in Thomas et al., 2019) may be key in differentiating sediment sources along the Laurentian margin. In the absence of a comprehensive auxiliary data set such as detrital zircon  $\epsilon\text{Hf}(t)$ , we use sediment provenance maps to make these interpretations (Fig. 8).

**Antler recycled.** Factorized source 5 exhibits a multimodal age distribution with a broad prominent positively skewed age mode at 1.8 Ga spanning much of the Paleoproterozoic. It also contains a minor Archean age mode (Fig. 5E). Factorized source 5 exhibits a very high correlation ( $R^2$ : 0.97) to early–middle Paleozoic sedimentary rocks exposed in thrust sheets of the Antler Orogen in southern Idaho (Beranek et al., 2016). These sedimentary rocks are interpreted to have a northerly source (e.g., Peace

River Arch of northwestern Alberta and north-eastern British Columbia, Canada; Gehrels and Pecha, 2014; Beranek et al., 2016). We interpret the presence of this source in upper Paleozoic rocks to represent recycled material shed from the intermittently collisional western margin of Laurentia (Trexler et al., 2004; Sturmer et al., 2018), particularly the northern segment.

**Early Paleozoic recycled.** Factorized source 11 exhibits a dominant Archean mode at ca. 2.71 Ga, contains minor Proterozoic age mode, and is highly correlated ( $R^2$ : 0.88) to Ordovician sandstones deposited from Michigan to Arkansas (USA) (Thomas et al., 2016) (Fig. 5F). This source is interpreted to primarily represent recycling of early Paleozoic strata. However, it could also be derived from the cratonic shield to the north; however, it is mostly attributed to quartz-rich and/or feldspar-poor strata (e.g., Vanoss Conglomerate; Thomas et al., 2016; Bushberg Sandstone; Chapman and Laskowski, 2019), which supports a recycled interpretation.

### Local Sources

**530 Ma basement.** Factorized source 10 is a ca. 530 Ma unimodal distribution that is highly correlated ( $R^2$ : 0.92) to Early Cambrian age igneous rocks (Fig. 5G) intruded into Laurentian crust during late-stage Rodinian rifting (McMillan and McLemore, 2004). These igneous rocks are best known for their exposure in southern Oklahoma as part of the exhumed ARM uplift. Other sites of Cambrian intrusion host igneous rocks of similar age occur across Colorado and New Mexico (McMillan and McLemore, 2004). We present zircon data from a Cambrian age syenite exposed in the Wet Mountains of Colorado and use this source to represent similar age rock exposed in basement or possibly sedimentary rocks sourced by that same basement and recycled from exhumed ARM uplifts.

**1.43 Ga basement.** Factorized source 8 contains a dominant ca. 1.43 Ga age mode and a minor ca. 1.73 Ga age mode (Fig. 5H), and exhibits a high correlation ( $R^2$ : 0.94) to granitic rock intruded into the Laurentian midcontinent (Bickford et al., 2015). These Mesoproterozoic igneous rocks are commonly referred to as anorogenic granites, but mounting evidence indicates that igneous emplacement during this time was associated with a protracted convergent margin along eastern Laurentia (Whitmeyer and Karlstrom, 2007; Bickford et al., 2015). This source is interpreted to reflect predominantly Mesoproterozoic granitoids that were intruded into Yavapai and Mazatzal basement and exhumed in western Laurentia during ARM deformation. Alternatively, attribution of this source could represent recycled detritus from earlier Paleozoic rocks that received sediment from these basement terranes.

**1.66 Ga basement.** Factorized source 1 exhibits a dominant ca. 1.66 Ga mode with a shoulder at ca. 1.53 Ga and a broad minor mode centered at ca. 1.33 Ga (Fig. 5I). The shoulder and minor mode are separated by a 1.43 Ga nadir that corresponds to factorized source 8 (1.43 Ga basement source described above; Fig. 5H). The Kingston Mining District gneiss exposed in central New Mexico (Amato and Becker, 2012) yields a high correlation to factorized source 6 ( $R^2$ : 0.81). We interpret ca. 1.66 Ga source to reflect detritus sourced by the Mazatzal terrane exposed predominantly in New Mexico during the late Paleozoic by ARM uplifts. This empirical source does not exhibit the minor 1.2–1.5 Ga age modes, which may contribute to misfits in top-down modeling (see the Discussion section).

**1.70 Ga basement.** Factorized source 6 is a ca. 1.70 Ga unimodal distribution that exhibits a very high correlation ( $R^2$ : 0.97) to the Caylor Gulch granodiorite exposed in the Front Range of Colorado (Guitreau et al., 2016) (Fig. 5J). This granodiorite is part of a broad suite of granitoid intrusions (1.72–1.68 Ga) that were emplaced during peak deformation of the Yavapai Orogeny (Whitmeyer and Karlstrom, 2007). We use the granodiorite sample to represent the abundant ca. 1.70 Ga age zircon source of the Yavapai basement terrane exhumed throughout the western interior during ARM deformation (Fig. 7).

**1.73 Ga basement.** Factorized source 4 contains a dominant ca. 1.74 Ga mode and a lesser 1.46 Ga mode that are both positively skewed (Fig. 5K). This factorization exhibits a moderate correlation ( $R^2$ : 0.65) to our empirical source match with a slightly younger age mode (ca. 1.73 Ga). We interpret this source to broadly represent Paleoproterozoic basement rocks of similar modal age in the Yavapai crustal terrane (Jessup et al., 2006; Whitmeyer and Karlstrom, 2007), which are commonly associated with minor intrusions of Mesoproterozoic igneous rocks. The limited multi-modal character of the factorized distribution, albeit not compensated for in our empirical sample, suggests common heterogeneity in the catchment exposing basement of this age, proximal downstream mixing, and/or recycling of local basement sourced sedimentary rock.

### Step 3. Top-Down Modeling

Top-down models generally yield greater misfit than bottom-up models when comparing mixed models and empirical samples (Fig. 6A). This is due to the imperfect matches of the empirical source set to the factorized sources and propagation of uncertainty in the match. The mean  $R^2$  between top-down mixed distributions and empirical samples presented above

is  $0.69 \pm 0.14$  ( $1\sigma$ ) and the median is 0.68. The mean Kuiper V value for these comparisons is  $0.19 \pm 0.08$  ( $1\sigma$ ) and the median is 0.16. Attribution of local sources between top-down  $R^2$  and Kuiper V models are highly correlated ( $R^2 = 0.92$ ; Fig. 6C). Comparison of  $R^2$ s for samples between bottom-up (DZnmf) and top-down (DZmix) indicate a poor correlation ( $R^2 = 0.46$ ). Despite this difference in the goodness of mixed model fits between top-down and bottom-up approaches, source attribution for individual samples is remarkably similar across both. This is illustrated by the high correlation of local source attribution of both top-down and bottom-up mixture models ( $R^2 = 0.85$ ; Fig. 6B). In other words, the mixing weight applied by the bottom-up and top-down approaches is similar, but the goodness of fit between sample and mixed distributions is not. In the case of top-down modeling, these results indicate a geologically realistic empirical source set that works well for sink data attribution, but one that would likely benefit by improving its fit to the factorized sources.

Basins within the ARM corridor exhibit an increase in the relative contribution of modeled local source attribution during ARM deformation (Fig. 2). However, presenting the results at the scale of a stratigraphic column, as in Figure 2, does not illustrate sediment fairways through time. We therefore complement this approach with a synoptic map view of these basins in the context of regional provenance trends.

### Step 4. Sediment Source Maps

To address the challenge of data visualization, we create provenance-contour maps that incorporate paleogeography, stratal thickness, and paleocurrent data. DZmix-modeled local source percentages are displayed next to data points (Fig. 8), which are shaded based on their goodness of fit ( $R^2$ ). These data and this approach provide geographic context for the changes in detrital zircon source identified in the following description of sediment provenance episodes. Maps shown in Figure 8 discriminate between local and distal sources and include symbols on data points that distinguish threshold contribution percentages for several distal sources (e.g., a light blue square that indicates >20% Antler recycled attribution).

## DISCUSSION

### Consideration of the Methods

Combining bottom-up and top-down modeling provides an effective approach to distill large detrital zircon data sets into a realistic

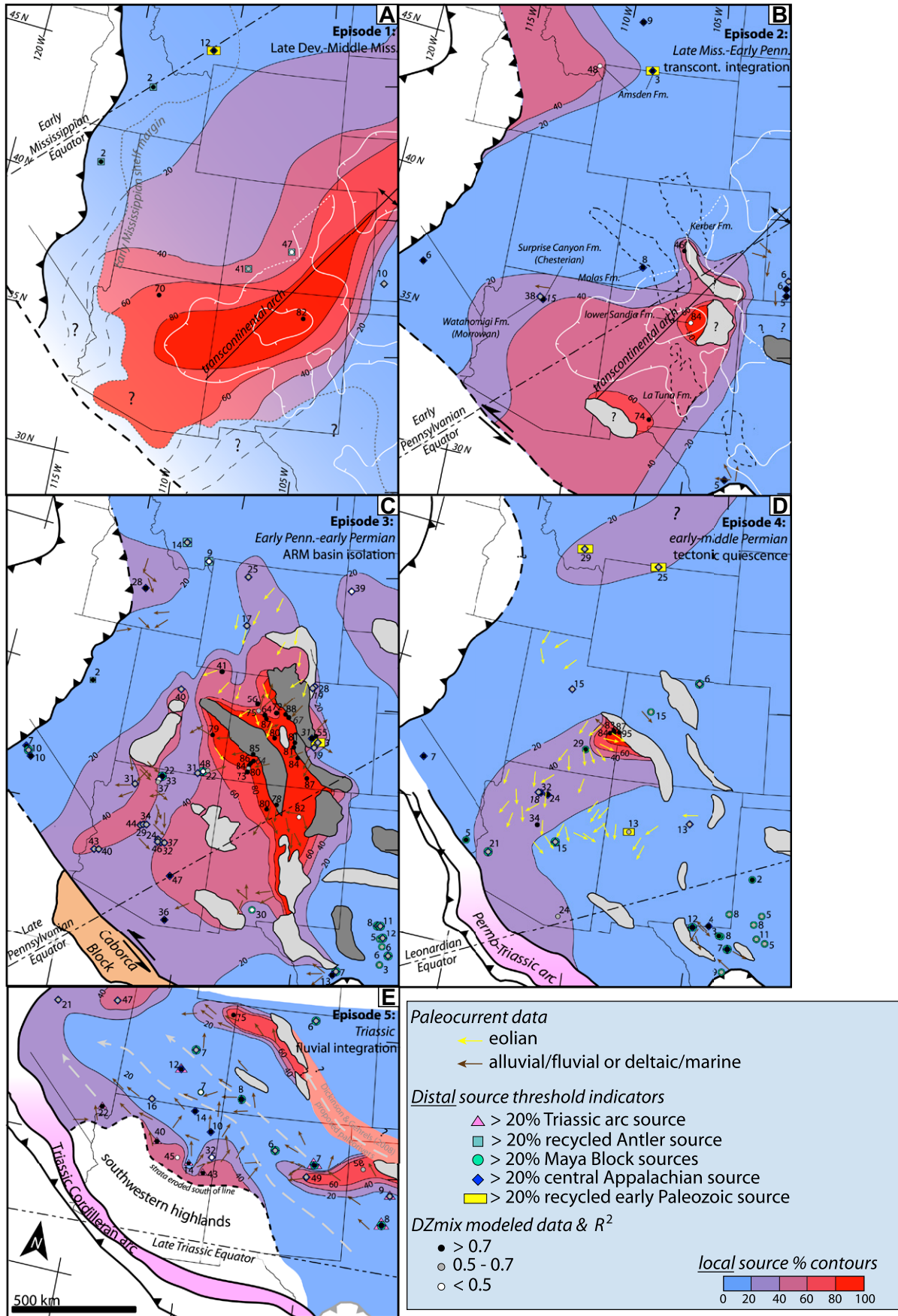


**Figure 8.** Sediment source maps for episodes 2–5 outlined in Figure 2 and discussed in the text (see Supplemental Material 1 for map of Episode 1). Data references used in maps are detailed in Supplemental Material 1. Red to blue coloring of source contour intervals helps illustrate local to distal source proportions that were attributed by top-down (DZmix) modeling to samples shown as shaded circles on the maps. These sample markers (i.e., data points) are shaded based on  $R^2$  (coefficient of determination or cross-correlation coefficient) value based on how similar the mixed models are to their corresponding sink samples. In other words, a measure of how well the top-down models matched the sample distributions. Number next to each data point indicates proportion of local source attribution. Several values are italicized, which indicate that the value was not used to contour because of a slight mismatch with surrounding data points (See the Discussion section in text). (A) Late Devonian (Dev.)–Middle Mississippian (Miss.) arch-controlled sedimentation episode. Sparse data on this map with large ranges in source percentages yield high uncertainty in drafting of contours. Paleogeography from Gehrels et al. (2011). Stratal thickness and zero Mississippian thickness line (white with tick marks) is from Carlson (1999). The tick marks indicate side of contour that marks the absence of stratigraphy. Note that in Figure 8B a modified version of this zero-thickness line is included, and that some of the areas of zero thickness are due to exhumation of the Ancestral Rocky Mountain (ARM) uplifts (i.e., after this episode). (B) Late Mississippian–Early Pennsylvanian (Penn.) transcontinental (transcont.) sediment integration episode. Zero-thickness line (Carlson, 1999) is modified to show what areas with no Mississippian strata are likely due to subsequent ARM exhumation. This provides the approximate position of the transcontinental arch leading into Episode 2. Paleogeography (Ye et al., 1996; Gehrels et al., 2011), and paleocurrent data (Billingsley, 1999; Bowen and Weimer, 2003; Gleason et al., 2007; Wang and Bidgoli, 2019). (C) Early Pennsylvanian–early Permian ARM basin tectonic isolation of sediment source episode. Paleogeography (Ye et al., 1996; Blakey, 2009; Gehrels et al., 2011; Lawton et al., 2017), stratal thickness maps (Ye et al., 1996; Blakey, 2009), and paleocurrent data (Opdyke and Runcorn, 1960; Johnson, 1987; Geslin, 1998; Soegaard and Caldwell, 1990; Eberth and Miall, 1991; Gleason et al., 2007; Sweet and Soreghan, 2010; Lawton et al., 2015; this study) were used in map construction. (D) Early Permian–middle Permian tectonic quiescence episode. Paleogeography (Loope et al., 2004; Leary et al., 2017), stratal thickness maps (Ewing, 1993; Ye et al., 1996), and paleocurrent data (McKee, 1940; Rea, 1967; Conyers, 1975; Adams, 1980; Loope et al., 2004; Lawton et al., 2015; Brand et al., 2015; Dickinson, 2018) were used in map construction. (E) Triassic Fluvial integration episode. Gray dashed arrows indicate paths of proposed Triassic paleorivers (Dickinson and Gehrels, 2008), which are displayed with a light red swath and question marks to indicate lack of confidence in the interpretation. Paleogeography (Dickinson and Gehrels, 2008; Lawton et al., 2018), stratal thickness maps (Dickinson and Gehrels, 2008; Kent and Irving, 2010), and paleocurrent data (Willis, 1967; Williams and Harms, 1988; Dickinson and Gehrels, 2008; Brand et al., 2015; Riggs et al., 2016; this study) were used in map construction. DZmix modeling results for all samples used in the construction of these maps are provided in the Supplemental Material 6. Latitude and longitude are provided in modern reference frame. See Supplemental Material 1 for cited paleogeography reference figures. Fm.—Formation.

empirical source set and assign source proportions (Fig. 3). Instead of describing each sample as discretized age bins, we approach detrital zircon age distributions as continuous functions, similar to seismic waves, and leverage the size of the data set to our interpretive advantage. However, source signals, or factorized sources, are only useful if they provide information that can be interpreted within a geologic context. This is where the iterative approach to identifying empirical sources and then comparing them to the factorized sources is particularly instructive. Top-down modeling also helps to mitigate bias. In the case of DZmix, it does so by randomly mixing known source inputs (a.k.a. the empirical source set) to produce a mixture model distribution. This modeled distribution is then compared to the actual detrital zircon age distribution to determine the best model fits. A benefit of using this approach over age binning of data is that the model can generally discriminate between sources containing the same non-unique ages based on the shape of the distribution and/or accompanying age modes. Moreover, it considers the proportions of those age modes. Combining bottom-up and top-down modeling helps to decrease bias, lay out an approach to source analysis for large provenance data sets, and provide guidance in sediment source identification and attribution.

However, the combined bottom-up and top-down approach is not without limitations. Despite developing an empirical source set that is very highly to moderately correlated (see definitions in Table 1) to the respective factorized sources (Fig. 5), top-down models yield a worse fit to samples than do bottom-up models (Fig. 6A). The greater misfit between top-down models and samples in comparison to bottom-up models is most likely due to the NMF algorithm attributing minor age modes to samples where they are absent in the empirical source samples. For example, factorized source 9 includes a minor age mode at ca. 1.46 Ga that is absent from the Triassic arc empirical sample (see the section Step 2. Comparison of Factorizations to Empirical Sources above). Nevertheless, correlation of source attribution between DZnmf and DZmix is high (i.e., mean  $R^2$  of source attribution is 0.87 and local source attribution  $R^2$  of 0.94; Fig. 6A). These metrics indicate high fidelity between source attribution of the two mixture modeling methods despite the worse top-down model fits. Further, these results suggest that uncertainties associated with mixed model-to-sample distribution comparisons, as well as factorized-to-empirical source comparisons propagate from bottom-up modeling to factorized-empirical source comparison and then to top-down modeling.

It follows that there is room for improvement in the empirical source set, as well as in the approach itself.

Bottom-up modeling, particularly with tools such as DZnmf, provides a clarifying approach to evaluate which detrital zircon sources play a critical role in the basin record, and which do not. For example, it may be troubling to some readers that we use only three source ages (1.66, 1.70, and 1.73 Ga; Figs. 5I–5K) to represent detrital zircons from the Yavapai and Mazatzal terranes, as they host a protracted assemblage of igneous ages that span 1.60–1.80 Ga (Whit-meyer and Karlstrom, 2007). However, these ages directly correspond to factorized age distributions constructed from an 11-source factorization (factorized sources 1, 6, and 4, respectively; Figs. 5I–5K) that exhibit high to very high correlation ( $R^2$  of  $0.90 \pm 0.08$  ( $1\sigma$ ) mean and 0.91 median) between sample and factorized model age distributions. In other words, the well correlated bottom-up model indicates that ages outside of the ones characterized in factorized sources 1, 6, and 4, but included in the Yavapai and Mazatzal terranes, were not major contributors to the sedimentary record examined here.

In some cases, non-unique age distributions remain an issue when applying these methods and point to the need for integrative data interpretation. In the case of discerning between

similar age distributions of basement versus recycled sources, use of sandstone petrography (i.e., quartz-rich versus feldspar-rich) is a straight-forward approach to aid in discriminating sources. For example, the Denver Basin shows a relatively low percent of local source relative to other ARM basins proximal to uplifts during Episode 3 (e.g., Central Colorado Trough (CCT), Taos Tough). Although these strata (i.e., the Fountain Formation) are arkosic (Suttner and Dutta, 1986), top-down modeling of the 11-source set yields surprisingly high distal source attribution. This is due to the absence of an age distribution correlative to the 1.085 Ga Pikes Peak Batholith, which was exhumed in the Ancestral Front Range, in the 11-source set. Previous research makes a compelling case for the source of Pennsylvanian–Permian strata in the Denver Basin (Fountain and Ingleside formations) to have been shed by the adjacent Ancestral Front Range (Sweet and Soreghan, 2010; Leary et al., 2020). In the absence of a 1.085 Ga source, DZmix selected the central Appalachian source (Fig. 5B) as the best match to Fountain and Ingleside formation samples. DZnmf factorizes out a 1.085 Ga age distribution in the 12-source factorization (Supplemental Material 5) and we experimented with re-mapping Episode 3 with DZmix results from an 11-source set plus a Pikes Peak source (Supplemental Materials 1 and 6). Improvement of the DZmix model fits for the Denver Basin samples were proportional to the percent of the 1.085 Ga source attributed. The most drastic change was observed in an arkosic Denver Basin sample (Fountain Formation 2 SG; Supplemental Material 2) where the model fit improved over  $2\sigma$  (from 0.58 to 0.91), central Appalachian source decreased (from 0.61 to 0.03), and 1.085 Ga source attribution was 0.84 (Supplemental Material 6). The provenance map contoured with modeled results from this alternate source set, which contains the 1.085 Ga source (Supplemental Material 1) shows that the Denver Basin appears to have a small area that was dominated by local sediment. The 11-source set model map in Figure 8C does not capture this. However, we decided not to include

the 1.085 Ga source in the source set presented here because it is a relatively minor source, and although its addition improves some of the Denver Basin samples, it appears to be erroneously attributed to other samples distant from the Pikes Peak batholith, albeit in low proportions (Supplemental Materials 1 and 6), thereby inflating the influence of local source attribution across a broad area. Therefore, we decided that on balance we could not justify the addition of this source to our source set given the scale of our provenance maps. Instead, we highlight this result as a potential shortfall of the approach we present here.

Source mapping, as presented here, provides a new method to visualize provenance data. This approach is different from previous attempts to map sediment sources (e.g., Wissink et al., 2016; Blum et al., 2017) in that we are not mapping proportions of binned ages, but rather proportions of sources which are themselves characterized by continuous functions. This approach also creates a synoptic view of provenance data that incorporates other geologic information (e.g., stratigraphic thickness, paleocurrents). Integration of additional data and hand-contouring yield a final product with an element of interpretation. Although this inherently introduces bias, it also facilitates interpretation of a larger, more diverse set of data. We use top-down modeled detrital zircon source contributions as the primary input; however, it would be possible to substitute these source proportions with one of many other quantitative or semiquantitative provenance proxies (e.g., proportions derived from clast-counts, bottom-up model source results, a selected binned age-group).

When creating a source map, data selection and filtering are of top importance and need to be customized to the purpose of the map. In the case presented here, the purpose is to investigate the distribution and magnitude of ARM-driven provenance in western Laurentia. Therefore, we lumped the modeled sediment sources into local or distal, contoured local source contribution with consideration of auxiliary data, and included threshold symbols for the dominant

distal sources (e.g., a pink triangle for samples with  $>20\%$  Triassic arc source attribution; Fig. 8).

The question of which data set is better to create source maps with, top-down or bottom-up modeled source proportions, is not addressed here. While we do not contour bottom-up results, local source attribution is highly correlated ( $R^2 = 0.94$ ) between DZmix and DZnmf models (Fig. 6B), indicating that source maps would be similar. However, the answer to which approach is better is likely contingent on the purpose of the map(s) one is contouring. The purpose of this paper is to evaluate the distribution of local sources around the ARM, and to introduce a new approach of handling, interpreting, and visualizing large provenance data sets. For the latter purpose, showing the loop of using basin samples to create bottom-up factorized sources that are then used to inform selection of real-rock sources, which, in turn, are used in top-down modeling, is valuable in demonstrating the range of possibilities in this approach. We also prefer the real-rock link between source and sink inherent in modeling with the top-down model results. However, bottom-up results exhibit less of a misfit than top-down results (mean DZnmf  $R^2 = 0.91$  versus mean DZmix  $R^2 = 0.70$ ; Supplemental Material 6), leaving us agnostic as to which is “better” to map with. Further, it may be reasonable to say that there is no purpose in compounding the misfit between factorized and real-rock sources by modeling with an inferior source set (i.e., empirical source set used in top-down modeling). We hope to see many applications of this new approach, and utilization of many different provenance data sets, and, in doing so, the applicability and best practices for it will be developed.

#### Comparison of Factorizations Presented in This Study and Leary et al. (2020)

Many of the factorized sources presented in this paper are similar to factorized sources presented in Leary et al. (2020), and most of our interpretations are similar as well (Table 2). However, a few sources presented here that exhibit similarity to Leary et al. (2020) sources are interpreted differently. For example, factorized sources 3 and 7 are interpreted here as Maya Block (or similar peri-Gondwana terrane) sources (Fig. 5). However, combined, these sources are similar to “Source A” from Leary et al. (2020), which was interpreted as a northern Appalachian source. The difference in our results, and therefore interpretations, is likely due to the expanded detrital zircon data set used here that includes additional new and previously published samples (Supplemental Material 2).

TABLE 2. DERITAL ZIRCON SOURCE INTERPRETATION COMPARISON: LEARY ET AL. (2020) AND THIS STUDY

Factorized source (this study)	Factorized source (Leary et al., 2020)	Interpreted empirical source (this study)	Interpreted empirical source (Leary et al., 2020)
9	n/a	Triassic arc	n/a
2	B	Central Appalachian	Central Appalachian
3 and 7	A	Maya Block	Northern Appalachian
5	C	Antler recycled	Antler recycled
11	E	Early Paleozoic recycled	Archean basement
10	H	530 Ma basement	531 Ma basement
8	G	1.43 Ga basement	1.43 Ga basement
1	D	1.66 Ga basement	Zuni Uplift or recycled Antler Orogen
6	F	1.70 Ga basement	1.70 Ga basement
4	n/a	1.73 Ga basement	n/a

Note: n/a—not applicable.

Factorized source 1, interpreted as 1.66 Ga basement, is similar to “Source D” in Leary et al. (2020), but lacks the 1.75 Ga mode and replaces the 1.1–1.4 Ga distribution with a minor peak at 1.35 Ga. We attribute the minor but clarifying differences in age distribution observed in factorized source 1 versus “Source D” to the larger size of the data set analyzed here, similar to the case mentioned above. This may have allowed the NMF algorithm to better characterize this source and/or further deconvolve a mixed “Source D” into its constituents. To this point, the primary recipients of factorized source 1 are several New Mexico samples that were added to our data set, but were not in the Leary et al. (2020) data set. With stated uncertainty, Leary et al. (2020) attributed “Source D” to either exhumation of the Zuni Uplift or recycling of foreland basin strata along an expanded Antler orogenic front. However, we favor a Mazatzal basement source interpretation, which underlies the Zuni Uplift.

### Western Laurentian Sediment Routing Episodes

We divide the Late Devonian–Triassic study interval into five episodes based on modeled sediment provenance trends and comparison to previously published literature (e.g., Dickinson and Gehrels, 2008; Gehrels et al., 2011; Chapman and Laskowski, 2019; Leary et al., 2020). Characterization of sediment provenance episodes is focused on the core ARM basins (Fig. 1), is defined by changes in the distribution of local versus distal sourced sediment, and reflects major changes in sediment routing and provenance in western Laurentia. These episodes include (1) arch-controlled sediment dispersal (Late Devonian–Middle Mississippian), (2) transcontinental sediment integration (Late Mississippian–Early Pennsylvanian), (3) ARM basin isolation (Early Pennsylvanian–early Permian), (4) tectonic quiescence and eolian sediment mixing (early Permian–middle Permian), and (5) transcontinental fluvial reintegration (Triassic: predominantly Late) (Fig. 2).

#### Episode 1: Arch-Controlled Sediment Dispersal

The eight samples and sample groups that comprise the Late Devonian–Middle Mississippian Episode 1 exhibit different detrital zircon age distributions based on their geographic location relative to the transcontinental arch (Fig. 8A). This pattern of sediment dispersal is documented as far back as the Cambro-Ordovician (Amato and Mack, 2012), the extent of which is outside the scope of this paper. During this interval western Laurentia received a mix

of local (i.e., Yavapai and Mazatzal crustal terrane) and distal (predominantly Antler recycled) sources. Age distributions to the east of the transcontinental arch (Figs. 2Civ and 2Cv; Supplemental Material 6), as well as those deposited on the Montana shelf are predominantly attributed to the central Appalachian source (Fig. 5B) with a significant contribution from the early Paleozoic recycled source (Fig. 5F). Samples that fall along the transcontinental arch (e.g., sandstones within the Leadville Limestone) are either dominated by local sources (e.g., incipient Taos Trough sample) or contain a mixture of local and Antler recycled sources. To the west of the arch, the White River and Ely basins (Fig. 1) appear to be dominated by the Antler recycled source (Fig. 5E). We favor a model of sediment compartmentalization across the transcontinental arch (Linde et al., 2014) with intermittent cross-arch connectivity during sea-level highs (Chapman and Laskowski, 2019) to explain provenance distribution observed in the data (Fig. 8A). We interpret the source of local sediment within the study area to be directly arch-derived or recycled from local sediment that itself was originally arch-derived.

#### Episode 2: Transcontinental Sediment Integration

Episode 2 marks a period of major sedimentation reorganization in western Laurentia during the Late Mississippian–Early Pennsylvanian (Chesterian–Morrowan) (Fig. 8B), but it is complicated by a protracted hiatus in the Late Mississippian (Chesterian). McKee and Crosby (1972, plate 2) show that most rock beneath Pennsylvanian stratigraphy in western North America is Middle Mississippian (Meramecian) and older, which highlights the paucity of Upper Mississippian (Chesterian) sedimentary rock throughout the study area. This subcrop pattern follows the trace of the transcontinental arch, indicating its persistence as a positive feature at least up to Early Pennsylvanian (Morrowan) (Blakey, 2009).

There is a rapid, but slightly diachronous change in provenance seen in Upper Mississippian–Lower Pennsylvanian strata from the Arizona shelf, Paradox Basin, and Montana shelf (e.g., the Molas and Surprise Canyon formations; Fig. 2). Upper Mississippian (Chesterian) fluvial-estuarine rocks (i.e., Surprise Canyon Formation) (Billingsley, 1999) record the introduction of Appalachian-sourced sediment to the western Laurentian margin (Gehrels et al., 2011) (Fig. 8A). However, this was followed within ~5 m.y. by an increase in local-source zircons in the Lower Pennsylvanian (Morrowan) marine strata (i.e., Watahomigi Formation) (Hodnett and Elliott, 2018) (Figs. 2 and 8B). With no fur-

ther context, these data could suggest that this increase in local provenance was due to early exhumation of ARM uplifts. However, Lower Pennsylvanian (Morrowan) fluvial deposits on the Montana shelf (i.e., Amsden Formation) and incipient Paradox Basin (i.e., Molas Formation, which stretches into the Atokan; Evans and Reed, 2007) exhibit similar facies, and detrital zircon age distributions as the Upper Mississippian (Chesterian) fluvial strata on the Arizona shelf (Fig. 8B). Like these fluvial Arizona shelf strata, the Lower Pennsylvanian fluvial deposits on the Montana shelf and Paradox Basin were deposited on top of karsted Mississippian carbonates. This observation spurs the question: Are these diachronous deposits related, and if so, how?

We interpret this diachronous package of fluvial rock to record progressive eastward infilling of incised fluvial valleys and onlap that developed on the complex-karsted topography of Mississippian limestones (Evans and Reed, 2007). The transgression was driven by a second order eustatic sea level rise that flooded vast continental areas in the earliest Pennsylvanian (Sloss, 1963; Vail and Thompson, 1977; Haq and Schutter, 2008). Local detrital zircon sources (1.66 and 1.70 Ga; Figs. 5I and 5J) observed in the marine Watahomigi Formation may indeed be a signal of early ARM exhumation (i.e., either from exposed basement or recycled from early Paleozoic strata), but are not from the area around the northern Uncompahgre Uplift. This can be extrapolated from the predominant distal source of detrital zircons in the approximately coeval fluvial rocks (i.e., Molas Formation) (Fig. 8B). Therefore, while fluvial systems that supplied the incipient Paradox Basin may have also delivered that distal sediment to the Arizona shelf, they did not transport locally derived sediment to it, or at least they did not until tapping basement sources downstream of the northern Paradox Basin area. Furthermore, most Paradox Basin samples receiving sediment from the Uncompahgre Uplift during the subsequent episode contain a significant component of 1.43 Ga source, which the marine rocks of the Arizona shelf (i.e., Watahomigi Formation) do not contain (Fig. 2 and Supplemental Material 6). Instead, during this time, we attribute local detritus identified in Arizona shelf strata to be from basement exposed either along the transcontinental arch or areas of early ARM exhumation (Fig. 8B), as unroofing of some ARM uplifts is documented during this time (e.g., Musgrave, 2003). This may include the southern portion of the Uncompahgre Uplift (also termed San Luis Uplift *sensu* Blakey, 2009).

The Episode 2 source map (Fig. 8B) depicts sediment dispersal systems controlled by the

transcontinental arch. Both during the Late Mississippian, when it served as a large area of non-deposition and karsting, and during the Morrowan, when sediment covered it as seas rose. It was also the approximate site of possible early ARM deformation (Leary et al., 2017; Sweet et al., 2021) and local sedimentation in a few basins (e.g., CCT; Musgrave, 2003). While it would be possible to route sediment around nascent ARM uplifts, the presence of a continental scale arch, at least until the Early Pennsylvanian (McKee and Crosby, 1972) would appear to be an impediment to central Appalachian sediment arriving on the western Laurentian margin in the Late Mississippian. Therefore, how would transcontinental sediment pass this barrier?

We offer several possible scenarios that describe how sediment could have been transported from the eastern to the western margin of Laurentia (modern reference) during this time. (1) A southwest-directed pathway that delivered Appalachian sediment from the northeast, which effectively routed detritus around the northern extent of the arch. (2) Pathways that intermittently transported sediment over the arch by ocean currents during higher frequency sea level rises (Chapman and Laskowski, 2019). (3) Pathways that delivered sediment were routed through paleovalleys that cut across the transcontinental arch, similar to, but with different orientation than Late Mississippian paleovalleys identified in western Kansas and eastern Colorado (Sonnenburg et al., 1990; Bowen and Weimer, 2003; Wang and Bidgoli, 2019). (4) Alternatively, Carlson (1999) suggests that the transcontinental arch was not a continuous feature, but rather a discontinuous platform consisting of a series of basement-cored features. In this scenario, sediment pathways could have utilized gaps in the arch that may have been enhanced, or even created by early subtle ARM deformation.

Integration of the continental-scale drainage system during Episode 2 was short-lived in the core of the ARM. Along the transcontinental arch, pockets of Lower Pennsylvanian (Morrowan) strata in the CCT, Taos Trough, and western Orogrande Basin received predominantly local sediment (Fig. 8B) contributed by 1.70 and 1.66 Ga sources. Unlike subsequent deposition in the Pennsylvanian, these initial sandstones are quartz-rich (DeVoto et al., 1971; Baltz and Meyers, 1999; Musgrave, 2003; Amato, 2019) and are interpreted to indicate recycling of lower Paleozoic strata from along exposed areas of the transcontinental arch and/or nascent ARM uplifts.

### Episode 3: Core ARM Basin Isolation

Episode 3 is defined by the dominance of local basement sediment deposition around core

ARM uplifts during the Early Pennsylvanian–early Permian (Atokan–Wolfcampian). The Paradox Basin, Eagle Basin, CCT, and Taos Trough contain large areas of  $\geq 80\%$  local source attribution. The Denver Basin appears to be an outlier regarding locally sourced sediment. However, although it is not as sedimentologically isolated as other nearby ARM basins, its uncharacteristically low local attribution illustrated in Figure 8C is in part an artifact of a shortcoming in the 11 source-set used to model it. This source set lacks the 1.085 Ga granitoid source, which is adjacent to the strata bearing this age zircon, and instead misattributes the Grenville-dominant central Appalachian source. For further detail of this misattribution, and why we decided not to include the 1.085 Ga source in the empirical source set applied here (Fig. 5), see the Consideration of the Methods section in the Discussion section above. Evidence of local-derived sediment in the Denver Basin resides in the Lower–Middle Pennsylvanian coarse-grain strata along the eastern basin margin, which document unroofing and subsequent arkosic sedimentation during this episode (Sweet and Soreghan, 2010). For the first time, the 1.43 Ga source (Fig. 5H) serves as a major contributor to the local source profile of many samples. Areas of local source attribution outside of core ARM basins expand to the northwest, commonly exhibiting 20%–50% local source attribution. The Arizona shelf is a mixing pot of local and distal sediment. It received distal sediment from a corridor to the northeast that appears to have transported detritus between the Emery and Piute uplifts to the west and the Uncompahgre Uplift to the east (Figs. 1 and 8C).

The prominence of basement uplifts as dominant sediment sources in the core of the ARM was not ubiquitous across all ARM basins. The Central Basin Platform, which separates the Delaware and Midland basins (Fig. 1), was only modestly emergent despite causing  $>2$  km of flexural subsidence in the adjacent Permian Basins (Yang and Dorobeck, 1995). Instead, it primarily served as a high-relief carbonate platform (Ewing, 1993) between the two deep Permian Basins (i.e., Delaware and Midland basins; Fig. 1). Therefore, it never became a major contributor of siliciclastic sediment during ARM deformation, and adjacent basins instead received siliciclastic sediment from distal sources. This example of an ARM basin where adjacent local (siliciclastic) sediment production was suppressed highlights the continued presence of distal detritus and suggests that core ARM basins were overfilled by locally derived sediment. Furthermore, source mapping of this episode (Fig. 8B) suggests that most of the overflow of local sediment from core ARM basins was predominantly transported west (e.g.,

Arizona shelf) rather than east (e.g., Permian Basin area).

During this episode distal sources continued to dominate sedimentation outside the core ARM. Transcontinental sediment delivery to areas around western Laurentia did not shut down during ARM deformation, but was likely routed around it. Recycled Antler (Fig. 5E) and Maya Block (Figs. 5C and 5D) source contributions were location dependent with the greatest proportions located along the western Laurentian margin and Midland Basin, respectively. In contrast, the central Appalachian source (Fig. 5B) contributed to samples across the study area. Northeast to southwest sediment pathways running through the Wyoming and Montana shelves, northern Utah, eastern Nevada, and southeastern California provided routes for abundant central Appalachian sediment. The close match between measured samples and mixture models that incorporate the central Appalachian source support the continued delivery of these zircons to western Laurentia during Episode 3. The recycled Antler source dominated samples from the Ely Basin and contributed notably to samples in southwest Montana. We interpret this to indicate the intermittent tectonic activity along the western Laurentian margin (Trexler et al., 2004; Sturmer et al., 2018). In west Texas, the Maya Block and central Appalachian sources dominated the Marathon and Midland basins. We acknowledge the possibility that the central Appalachian source attribution in these samples may instead represent a similar Grenville age population contributed by peri-Gondwanan terranes to the south (e.g., Coahuila terrane as suggested by Thomas et al., 2019). In fact, Wolfcampian samples tend to exhibit poorer model fits. However, regardless of eastern or southern orogenic source, provenance mapping in this area offers a second possible distal source pathway into western Laurentia (i.e., from the southwest), although data are scant in the southwest during this episode.

### Episode 4: Tectonic Quiescence and Eolian Sediment Mixing

Episode 4 is defined by an increase in eolian deposition (Blakey, 2008; Lawton et al., 2015) and a decrease in local sources throughout most of western Laurentia during the early–middle Permian (Leonardian–Guadalupian) (Fig. 8D). These changes are associated with waning ARM tectonics (Blakey, 2008) and an increasing aridity (Crowell, 1999; Preto et al., 2010; Lawton et al., 2021). This combination of factors facilitated increased mixing of abundant distal sources and limited local sources (Lawton et al., 2015, 2021), and homogenized the provenance signal across western Laurentia. The northern Paradox Basin appears to be the only



exception as the Leonardian upper Cutler Formation (Trudgill et al., 2011) exhibits high local source attribution. This may be due to late-stage ARM exhumation of the northern Uncompahgre Uplift (Blakey, 2009). Across the rest of western Laurentia, samples and sample groups indicate <35% local attribution. Higher local sediment attribution occurs in a curved, mostly longitudinal band, and appears to come from the Uncompahgre Uplift. It is important to note that the data used to draw the contours that illustrate the longitudinal band are sparse, and one could imagine filling in the empty space on the map (Fig. 8D) with a different shape than is shown. The 1.43 Ga source (Fig. 5H) is dominant in the proximal northern Paradox Basin. However, the 1.66 Ga (Fig. 5I) source constitutes most of the local source attribution along the curved band. This may reflect a basement-derived detrital zircon age from the Uncompahgre Uplift that is not captured by regional basement maps (Whitmer and Karlstrom, 2007) (Fig. 7), sediment from another exposed remnant ARM uplift along that band (e.g., Zuni Uplift: Fig. 1), and/or recycling of recently deposited sediment (i.e., deposits from Episode 2).

Central Appalachian (Fig. 5B) and Maya Block sources (Figs. 5C and 5D) constitute the predominant distal sources, whereas the early Paleozoic recycled source (Fig. 5F) is present in a few samples, most of which are on the Wyoming and Montana shelves. Central Appalachian sourcing was the dominant distal source for a large area extending westward from  $\sim 105^\circ\text{W}$  (present-day coordinates). The dominant distal source in the southeastern corner of the study area was the Maya Block, which is consistent with the location of the Midland, Delaware, and Marathon basins adjacent to peri-Gondwanan terranes. However, attribution of this source farther north is at odds with most fluvial and eolian paleocurrent data, which indicate southward sediment transport (Fig. 8D). We interpret this to indicate that either paleocurrent measurements presented here do not fully capture sediment transport direction during this episode, or that Maya Block attribution is serving as a surrogate for similar detrital zircon age distributions in the Appalachian Mountains (e.g., Kissock et al., 2018).

### **Episode 5: Transcontinental Fluvial Integration**

Episode 5 is separated from the early–middle Permian eolian sediment mixing by unconformities in Utah, Colorado, New Mexico, and Arizona (McKee and Oriel, 1967), and is marked by a return to fluvial-dominated deposition. This sediment transport system delivered detritus across Laurentia (Lawton, 1994; Dickinson and

Gehrels, 2008), connecting the relict collisional margin of the Ouachita-Marathon Mountains to the Nevada shelf (Dickinson and Gehrels, 2008). These Triassic depositional systems span from the Sonoma Orogeny in Nevada to the initial development of the Cordilleran arc (Fig. 2) (Lawton, 1994), thereby marking another major change in tectonic regime and sediment transport in western Laurentia. Although this episode is broadly distinguished as Triassic, the data displayed in the source map (Fig. 8E) are mostly Late Triassic, and are therefore representative of that time. Due to a paucity of data from Lower–Middle Triassic Moenkopi Formation and equivalent strata, we combined these data with the abundant Late Triassic data.

The source map for Episode 5 (Fig. 8E) illustrates fluvial systems that connected the relict collisional margin of the Ouachita-Marathon Mountains to the Nevada continental shelf (Dickinson and Gehrels, 2008). Modeled samples exhibiting high distal source attribution stretch from southeast to northwest across western Laurentia (Fig. 8E). The Triassic arc source (Fig. 5A), for the first time, was a notable contributor to some detrital zircon samples along the southwestern Laurentian margin. The digitate pattern of Triassic arc attribution exhibited by samples along the southwestern highlands highlights the variability of provenance in these transverse fluvial drainages interacting with the trunk system that flowed to the northwest (Fig. 8E). Local sources along the southwestern margin of the study area are predominantly attributed to 1.43 Ga basement. The central Appalachian (Fig. 5B) and Maya Block (Figs. 5C and 5D) were the dominant distal sources, whereas the Antler recycled (Fig. 5E) and early Paleozoic recycled (Fig. 5F) sources were relatively minor contributors. Areas with high proportions of local sources appear to extend in tongues, east-to-west and southeast-to-northwest from basement sources that are inferred to have been exposed at this time (Dickinson, 2018). For example, the tongue which extends from southwestern Oklahoma is dominated by the 530 Ma source (Fig. 5G) and is most likely from the Amarillo Wichita Uplift (AWU) (Riggs et al., 1996; Dickinson and Gehrels, 2008).

While we favor the AWU as the most likely source of Cambrian detrital zircons in northern Texas and eastern New Mexico, we propose a possible alternative source for the northeastern Utah sample. It is possible that this sample was instead sourced by either Cambrian age igneous rocks still exposed in parts of the largely buried Ancestral Front Range, or by Pennsylvanian–Permian CCT strata that were themselves sourced from those same Cambrian rocks. Recent provenance work reveals that Pennsylvanian–Permian strata in this area were, at times,

exclusively sourced by proximal Cambrian rocks (Smith et al., 2023). The exclusivity of these Cambrian detrital zircons in some CCT strata demonstrate potential significance of Cambrian age igneous rocks and recycled sedimentary rocks west of the AWU as sediment contributors. The source map for Episode 5 (Fig. 8E) illustrates these two hypotheses by including a red swath across an area of no data to depict a possible sediment pathway from the AWU (as proposed by Dickinson and Gehrels, 2008). Alternatively, the map also includes a few areas of the remnant Ancestral Front Range uplift to indicate possible sourcing from a more proximal region.

## **CONCLUSIONS**

We present two novel elements for interpreting large detrital zircon geochronology data sets. (1) Combination of bottom-up and top-down source modeling, and (2) sediment-source mapping. The first approach leverages large data sets and source modeling to provide guidance in developing a vetted empirical source set and determining source attribution for large detrital zircon data sets (Fig. 3), rather than focusing on lengthy descriptions of binned age groups. While the data set used here is large, when filtered for time intervals of interest and plotted on maps, large areas contain no data, whereas others are densely populated. Source mapping is an integrative and interpretive approach that addresses this data distribution heterogeneity, aiding in geographic visualization of sediment dispersal systems, and demonstrating the utility of this approach across areas of sparse data. As with other geological applications, where data are limited, creation of contour plots allow extrapolation in a way that honors available data.

We applied these techniques to a late Paleozoic–early Mesozoic Laurentian data set and show that 191 samples and sample groups (created from 329 samples) can be factorized into 11 sources for which real examples (i.e., empirical sources) can be found. Contour mapping of top-down mixture model results and synthesis of previously published data reveal that western Laurentia experienced five episodes of sedimentation defined by changes in provenance and sediment routing particularly around the core of the ARM (Fig. 1). These include: (1) arch-controlled sediment dispersal (Late Devonian–Middle Mississippian), (2) transcontinental sediment integration (Late Mississippian–Early Pennsylvanian), (3) ARM basin isolation (Early Pennsylvanian–early Permian), (4) tectonic quiescence and eolian sediment mixing (early Permian–middle Permian), and (5) transcontinental fluvial

reintegration (Triassic: predominantly Late). Source maps uniquely reveal the degree and extent of ARM-associated tectonically driven source isolation. Furthermore, areas of intraplate deformation diverted transcontinental sediment dispersal systems around affected areas but did not shut those dispersal systems off. Sediment source modeling and provenance mapping indicate that influx of central Appalachian sediment from the northeast remained relatively consistent in the late Paleozoic. Beginning in Episode 3, Maya Block sources began to dominate provenance signatures inboard of the Marathon fold and thrust belt. The Triassic ushered in a new episode of transcontinental sediment dispersal, this time from the south and southeast, which included magmatic arc material.

#### ACKNOWLEDGMENTS

Funding for field and lab work, as well as publication costs, was provided by National Science Foundation (EAR-1824557), and graduate students grants from American Association of Petroleum Geologists, Geological Society of America, Sigma Xi, the University of Houston (UH), and University of British Columbia. Many thanks to field assistants Lokin Casturi, Crystal Saadeh, Kenny Lambert, and Noah Karsky. Special thanks to Minako Righter and Yongjun Gao for assisting with the U-Pb analyses and maintaining the UH laser-ablation-inductively coupled plasma-mass spectrometry lab facilities, to Tim Lawton, Bill Thomas, Scott Ryan, and two unnamed reviewers for their insightful and constructive reviews on this and/or earlier versions of this manuscript, to Tim Kusky, associate editor, for comments and guidance, and to Don Rasmussen for sharing his decades of experience in the Paradox Basin of western Colorado and Utah (USA). Thanks to James Hagadorn and Christopher Holm-Denoma for assistance navigating the U.S. Geological Survey data repository.

#### REFERENCES CITED

- Adams, R.D., 1980, Late Paleozoic tectonic and sedimentologic history of the Penasco Uplift, north-central New Mexico [M.A. thesis]: Houston, Rice University, 87 p.
- Amato, J.M., 2019, Detrital zircon ages from Proterozoic, Paleozoic, and Cretaceous clastic strata in southern New Mexico, U.S.A.: *Rocky Mountain Geology*, v. 54, no. 1, p. 19–32, <https://doi.org/10.24872/rmgjournal.54.1.19>.
- Amato, J.M., and Becker, T., 2012, Proterozoic rocks of the Caballo Mountains and Kingston mining district: U-Pb geochronology and correlations within the Mazatzal Province of southern New Mexico: *New Mexico Geological Society Guidebook*, v. 63, p. 227–234, <https://doi.org/10.56577/FFC-63.227>.
- Amato, J.M., and Mack, G.H., 2012, Detrital zircon geochronology from the Cambrian-Ordovician Bliss Sandstone, New Mexico: Evidence for contrasting Grenville-age and Cambrian sources on opposite sides of the Transcontinental Arch: *Geological Society of America Bulletin*, v. 124, no. 11–12, p. 1826–1840, <https://doi.org/10.1130/B30657.1>.
- Amidon, W.H., Burbank, D.W., and Gehrels, G.E., 2005, Construction of detrital mineral populations: Insights from mixing of U-Pb zircon ages in Himalayan rivers: *Basin Research*, v. 17, p. 463–485, <https://doi.org/10.1111/j.1365-2117.2005.00279.x>.
- Anfinson, O.A., Leier, A.L., Embry, A.F., and Dewing, K., 2012, Detrital zircon geochronology and provenance of the Neoproterozoic to Late Devonian Franklinian Basin, Canadian Arctic Islands: *Geological Society of America Bulletin*, v. 124, no. 3–4, p. 415–430, <https://doi.org/10.1130/B30503.1>.
- Aretz, M., Herbig, H.G., Wang, X.D., Gradstein, F.M., Agterberg, F.P., and Ogg, J.G., 2020, The Carboniferous Period, in Gradstein, F.M., Ogg, J.G., Schmitz, M., Ogg, G.M., eds., *Geologic Time Scale 2020*: Amsterdam, Elsevier, p. 811–874, <https://doi.org/10.1016/B978-0-12-824360-2.00023-1>.
- Attia, S., Paterson, S.R., Cao, W., Chapman, A.D., Saleeby, J., Dunne, G.C., Stevens, C.H., and Memeti, V., 2018, Late Paleozoic tectonic assembly of the Sierra Nevada prebatholithic framework and western Laurentian provenance links based on synthesized detrital zircon geochronology, in Ingersoll, R.V., Lawton, T.F., and Graham, S.A., eds., *Tectonics, Sedimentary Basins, and Provenance: A Celebration of the Career of William R. Dickinson*: Geological Society of America Special Paper 540, p. 268–296, [https://doi.org/10.1130/2018.2540\(12\)](https://doi.org/10.1130/2018.2540(12)).
- Baltz, E.H., and Meyers, D.A., 1999, Stratigraphic framework of upper Paleozoic rocks, southeastern Sangre de Cristo Mountains, New Mexico, with a section on speculations and implications for regional interpretation of Ancestral Rocky Mountains paleotectonics: *New Mexico Bureau of Mines and Mineral Resources Memoir* 48, 269 p.
- Barbeau, D.L., 2003, A flexural model for the Paradox Basin: implications for the tectonics of the Ancestral Rocky Mountains: *Basin Research*, v. 15, no. 1, p. 97–115, <https://doi.org/10.1046/j.1365-2117.2003.00194.x>.
- Beranek, L.P., Mortensen, J.K., Lane, L.S., Allen, T.L., Fraser, T.A., Hadlari, T., and Zantvoort, W.G., 2010, Detrital zircon geochronology of the western Ellesmerian clastic wedge, northwestern Canada: Insights on Arctic tectonics and the evolution of the northern Cordilleran miogeoclinal: *Geological Society of America Bulletin*, v. 122, p. 1899–1911, <https://doi.org/10.1130/B30120.1>.
- Beranek, L.P., Link, P.K., and Fanning, C.M., 2016, Detrital zircon record of mid-Paleozoic convergent margin activity U.S. Rocky Mountains: Implications for the Antler Orogeny and early evolution of the North American Cordillera: *Lithosphere*, v. 8, p. 533–550, <https://doi.org/10.1130/L557.1>.
- Bickford, M., Van Schmus, W.R., Karlstrom, K.E., Mueller, P.A., and Kamenov, G.D., 2015, Mesoproterozoic-trans-Laurentian magmatism: A synthesis of continent-wide age distributions, new SIMS U-Pb ages, zircon saturation temperatures, and Hf and Nd isotopic compositions: *Precambrian Research*, v. 265, p. 286–312, <https://doi.org/10.1016/j.precamres.2014.11.024>.
- Billingsley, G.H., 1999, Paleovalleys of the Surprise Canyon Formation in Grand Canyon, in Billingsley, G.H., and Beus, S.S., eds., *Geology of the Surprise Canyon Formation of the Grand Canyon, Arizona*: Flagstaff, Museum of Northern Arizona Bulletin 61, p. 17–52.
- Blakey, R.C., 2008, Pennsylvanian–Jurassic sedimentary basins of the Colorado Plateau and southern Rocky Mountains, in Miall, A.D., ed., *Sedimentary Basins of the World*: Amsterdam, Elsevier, v. 5, p. 245–296.
- Blakey, R.C., 2009, Paleogeography and geologic history of the Western Ancestral Rocky Mountains, Pennsylvanian–Permian, southern Rocky Mountains and Colorado Plateau, in Houston, W.S., Wray, L.L., and Moreland, P.G., eds., *The Paradox Basin Revisited: New Developments in Petroleum Systems and Basin Analysis*: Denver, Rocky Mountain Association of Geologists Special Publication, p. 222–264.
- Blakey, R.C., 2019, Pennsylvanian–Jurassic sedimentary basins of the Colorado Plateau and southern Rocky Mountains, in Miall, A.D., ed., *Sedimentary Basins of the United States and Canada*: Amsterdam, Elsevier, p. 315–367, <https://doi.org/10.1016/B978-0-444-63895-3.00007-3>.
- Blum, M.D., Milliken, K.T., Pecha, M.A., Snedden, J.W., Frederick, B.C., and Galloway, W.E., 2017, Detrital-zircon records of Cenomanian, Paleocene, and Oligocene Gulf of Mexico drainage integration and sediment routing: Implications for scales of basin-floor fans: *Geosphere*, v. 13, no. 6, p. 2169–2205, <https://doi.org/10.1130/GES01410.1>.
- Bowen, D.W., and Weimer, P., 2003, Regional sequence stratigraphic setting and reservoir geology of Morrow incised-valley sandstones (lower Pennsylvanian), eastern Colorado and western Kansas: *AAPG Bulletin*, v. 87, no. 5, p. 781–815, <https://doi.org/10.1306/08010201131>.
- Brand, L., Wang, M., and Chadwick, A., 2015, Data from: Global database of paleocurrent trends through the Phanerozoic and Precambrian: *Dryad, Dataset*, <https://doi.org/10.5061/dryad.hr0sp>.
- Brewer, J.A., Good, R., Oliver, J.E., Brown, L.D., and Kaufman, S., 1983, COCORP profiling across the Southern Oklahoma Aulacogen: Overthrusting of the Wichita Mountains and compression within the Anadarko Basin: *Geology*, v. 11, p. 109–114, [https://doi.org/10.1130/0091-7613\(1983\)11<109:CPATSO>2.0.CO;2](https://doi.org/10.1130/0091-7613(1983)11<109:CPATSO>2.0.CO;2).
- Capaldi, T.N., Horton, B.K., McKenzie, N.R., Stockli, D.F., and Odlum, M.O., 2017, Sediment provenance in contractional orogens: The detrital zircon record from modern rivers in the Andean fold-thrust belt and foreland basin of western Argentina: *Earth and Planetary Science Letters*, v. 479, p. 83–97, <https://doi.org/10.1016/j.epsl.2017.09.001>.
- Carlson, M.P., 1999, Transcontinental Arch: A pattern formed by rejuvenation of local features across central North America: *Tectonophysics*, v. 305, p. 225–233, [https://doi.org/10.1016/S0040-1951\(99\)00005-0](https://doi.org/10.1016/S0040-1951(99)00005-0).
- Cecil, M.R., Ferrer, M.A., Riggs, N.R., Marsaglia, K., Kylander-Clark, A., Ducea, M.N., and Stone, P., 2018, Early arc development recorded in Permian–Triassic plutons of the northern Mojave Desert region, California: *Geological Society of America Bulletin*, v. 131, p. 749–765, <https://doi.org/10.1130/B31963.1>.
- Chapman, A.D., and Laskowski, A.K., 2019, Detrital zircon U-Pb data reveal a Mississippian sediment dispersal network originating in the Appalachian Orogen, traversing North America along its southern shelf, and reaching as far as the southwest United States: *Lithosphere*, v. 11, no. 4, p. 581–587, <https://doi.org/10.1130/L1068.1>.
- Chestnut, D.R., and Greb, S.F., 2009, The Mississippian of the Appalachian Basin, in Greb, S.F., and Chestnut, D.R., eds., *Carboniferous Geology and Biostratigraphy of the Appalachian Basin*: Kentucky Geological Survey Special Publication 10, p. 22–31.
- Clark, C., Collins, A.S., Taylor, R.J., and Hand, M., 2020, Isotopic systematics of zircon indicate an African affinity for the rocks of southernmost India: *Scientific Reports*, v. 10, no. 1, p. 1–12, <https://doi.org/10.1038/s41598-020-62075-y>.
- Condon, S.M., 1995, Geology of Pre-Pennsylvanian rocks in the Paradox Basin and adjacent areas, southeastern Utah and southwestern Colorado: *U.S. Geological Survey Bulletin* 2000-G, 53 p.
- Conyers, L.B., 1975, Depositional environments of the Supai Formation in Central Arizona [M.S. thesis]: Tempe, Arizona State University, 86 p.
- Craddock, J.P., Malone, D.H., Porter, R., Compton, J., Luczaj, J., Konstantinou, A., Day, J.E., and Johnston, S.T., 2017, Paleozoic reactivation structures in the Appalachian-Ouachita-Marathon foreland: Far-field deformation across Pangea: *Earth-Science Reviews*, v. 169, p. 1–34, <https://doi.org/10.1016/j.earscirev.2017.04.002>.
- Crowell, J.C., 1999, Pre-Mesozoic ice ages: Their bearing on understanding the climate system: *Geological Society of America Memoir* 192, 106 p., <https://doi.org/10.1130/0-8137-1192-4.1>.
- De Voto, R.H., Peel, F.A., and Pierce, W.H., 1971, Pennsylvanian and Permian stratigraphy, tectonism, and history, northern Sangre de Cristo Range, Colorado, in James, H.L., ed., *New Mexico Geological Society, 22nd Annual Fall Field Conference Guidebook*, p. 141–163.
- Dickinson, W.R., 2018, Tectonosedimentary relations of Pennsylvanian to Jurassic strata on the Colorado Plateau: *The Geological Society of America Special Paper* 533, 184 p., <https://doi.org/10.1130/SPE533>.
- Dickinson, W.R., and Gehrels, G.E., 2008, U-Pb ages of detrital zircons in relationship to paleogeography: Triassic paleodrainage networks and sediment dispersal across southwest Laurentia: *Journal of Sedimentary Research*, v. 78, p. 745–764, <https://doi.org/10.2110/jsr.2008.088>.
- Dickinson, W.R., and Lawton, T.F., 2001, Carboniferous to Cretaceous assembly and fragmentation

- Mexico: Geological Society of America Bulletin, v. 113, no. 9, p. 1142–1160, [https://doi.org/10.1130/0016-7606\(2001\)113<1142:CTCAAF>2.0.CO;2](https://doi.org/10.1130/0016-7606(2001)113<1142:CTCAAF>2.0.CO;2).
- Dickinson, W.R., and Lawton, T.F., 2003, Sequential intercontinental suturing as the ultimate control for Pennsylvanian Ancestral Rocky Mountains deformation: *Geology*, v. 31, no. 7, p. 609–612, [https://doi.org/10.1130/0091-7613\(2003\)031<0609:SISATU>2.0.CO;2](https://doi.org/10.1130/0091-7613(2003)031<0609:SISATU>2.0.CO;2).
- Dickinson, W.R., Gehrels, G.E., and Stern, R.J., 2010, Late Triassic Mexico uplift preceding Jurassic opening of the Gulf of Mexico: Evidence from U-Pb ages of detrital zircons: *Geosphere*, v. 6, no. 5, p. 641–662, <https://doi.org/10.1130/GES00532.1>.
- Donaldson, A.C., Renton, J.J., and Presley, M.W., 1985, Pennsylvanian deposystems and paleoclimates of the Appalachians, in Phillips, T.L., and Cecil, C.B., eds., *Paleoclimatic Controls on Coal Resources of the Pennsylvanian System of North America: International Journal of Coal Geology*, v. 5, p. 167–193, [https://doi.org/10.1016/0166-5162\(85\)90013-8](https://doi.org/10.1016/0166-5162(85)90013-8).
- Dubiel, R.F., and Hasiotis, S.T., 2011, Depositional, paleosols, and climatic variability in a continental system: The upper Triassic Chinle Formation, Colorado Plateau, USA, in Davidson, S.K., North, C.P., and Leleu, S., eds., *From River to Rock Record: The Preservation of Fluvial Sediments and their Subsequent Interpretation: Society for Sedimentary Geology Special Publication*, v. 97, p. 393–421.
- Eberth, D.A., and Miall, A.D., 1991, Stratigraphy, sedimentology and evolution of a vertebrate-bearing, braided to anastomosed fluvial system, Cutler Formation (Permian-Pennsylvanian), north-central New Mexico: *Sedimentary Geology*, v. 72, p. 225–252, [https://doi.org/10.1016/0037-0738\(91\)90013-4](https://doi.org/10.1016/0037-0738(91)90013-4).
- Eble, C.F., Bascombe, B.M., Gillespie, W.H., and Pfefferkorn, H.W., 2009, Appalachian Basin fossil floras, in Greb, S.F., and Chestnut, D.R., eds., *Carboniferous Geology and Biostratigraphy of the Appalachian Basin: Kentucky Geological Survey Special Publication* 10, p. 46–58.
- Evans, J.E., and Reed, J.M., 2007, Integrated loessite-paleokarst depositional system, early Pennsylvanian Molas Formation, Paradox Basin, southwestern Colorado, U.S.A: *Sedimentary Geology*, v. 195, p. 161–181, <https://doi.org/10.1016/j.sedgeo.2006.07.010>.
- Ewing, T.E., 1993, Erosional margins and patterns of subsidence in the late Paleozoic west Texas basin and adjoining basins of west Texas and New Mexico: *New Mexico Geological Society Guidebook, Carlsbad Region, New Mexico and Texas, 44th Field Conference*, p. 155–166.
- Frahme, C.W., and Vaughn, E.B., 1983, Paleozoic geology and seismic stratigraphy of the northern Uncompahgre Front, Grand County, Utah, in Lowell, J.D., and Gries, R., eds., *Rocky Mountain Foreland Basins and Uplifts: Rocky Mountain Association of Geologists*, p. 201–211.
- Gao, Z., Perez, N.D., Miller, B., and Pope, M.C., 2020, Competing sediment sources during Paleozoic closure of the Marathon-Ouachita remnant ocean basin: *Geological Society of America Bulletin*, v. 132, p. 3–16, <https://doi.org/10.1130/B35201.1>.
- Gehrels, G., 2014, Detrital zircon U-Pb geochronology applied to tectonics: *Annual Review of Earth and Planetary Sciences*, v. 42, p. 127–149, <https://doi.org/10.1146/annurev-earth-050212-124012>.
- Gehrels, G.E., Blakey, R., Karlstrom, K.E., Timmons, J.M., Dickinson, B., and Pecha, M., 2011, Detrital zircon U-Pb geochronology of Paleozoic strata in the Grand Canyon, Arizona: *Lithosphere*, v. 3, no. 3, p. 183–200, <https://doi.org/10.1130/L121.1>.
- Gehrels, G.E., and Pecha, M., 2014, Detrital zircon U-Pb geochronology and Hf isotope geochemistry of Paleozoic and Triassic passive margin strata of western North America: *Geosphere*, v. 10, no. 1, p. 49–65, <https://doi.org/10.1130/GES00889.1>.
- Geslin, J.K., 1998, Distal Ancestral Rocky Mountains tectonism: Evolution of the Pennsylvanian-Permian Quirrh-Wood River Basin, southern Idaho: *Geological Society of America Bulletin*, v. 110, no. 5, p. 644–663, [https://doi.org/10.1130/0016-7606\(1998\)110<0644:DARMTE>2.3.CO;2](https://doi.org/10.1130/0016-7606(1998)110<0644:DARMTE>2.3.CO;2).
- Giannini, G.L., and Miskell-Gerhardt, K.J., 2009, Progradational mixed siliciclastic/carbonate sequence sets on the tectonically active eastern margin of the Pennsylvanian Paradox Basin, southwestern Colorado, in Houston, W.S., Wray, L.L., and Moreland, P.G., eds., *The Paradox Basin: New Developments in Petroleum Systems and Basin Analysis*: Denver, Colorado, USA, Rocky Mountain Association of Geologists Special Publication, p. 310–380.
- Gleason, J.D., Gehrels, G.E., Dickinson, W.R., Patchett, P.J., and Kring, D.A., 2007, Laurentian sources for detrital zircon grains in turbidite and deltaic sandstones of the Pennsylvanian Haymond Formation, Marathon Assemblage, west Texas, U.S.A: *Journal of Sedimentary Research*, v. 77, p. 888–900, <https://doi.org/10.2110/jsr.2007.084>.
- Guitreau, G., Mukasa, S.B., Blichert-Toft, J., and Fahnestock, M.F., 2016, Pikes Peak batholith (Colorado, USA) revisited: A SIMS and LA-ICP-MS study of zircon U-Pb ages combined with solution Hf isotopic compositions: *Precambrian Research*, v. 280, p. 179–194, <https://doi.org/10.1016/j.precamres.2016.05.001>.
- Harms, J.C., and Williamson, C.R., 1988, Deep-water density current deposits of Delaware Mountain Group (Permian), Delaware Basin, Texas and New Mexico: *The American Association of Petroleum Geologists Bulletin*, v. 72, p. 299–317.
- Haq, B.U., and Schutter, S.R., 2008, A chronology of Paleozoic sea-level change: *Science*, v. 322, p. 64–68, <https://doi.org/10.1126/science.1161648>.
- Hatcher, R.D., 2010, The Appalachian orogen: A brief summary, in Tollo, R.P., Bartholomew, M.J., Hibbard, J.P., and Karabinos, P.M., eds., *From Rodinia to Pangea: The Lithotectonic Record of the Appalachian Region: Geological Society of America Memoir* 206, p. 1–19, [https://doi.org/10.1130/2010.1206\(01\)](https://doi.org/10.1130/2010.1206(01)).
- Henderson, C.M., and Shen, S.Z., 2020, The Permian Period, in Gradstein, F.M., Ogg, J.G., Schmitz, M., and Ogg, G.M., eds., *Geologic Time Scale 2020*: Amsterdam, Elsevier, p. 875–902, <https://doi.org/10.1016/B978-0-12-824360-2.00024-3>.
- Hervé, F., Fanning, C.M., and Pankhurst, R.J., 2003, Detrital zircon age patterns and provenance of the metamorphic complexes of southern Chile: *Journal of South American Earth Sciences*, v. 16, no. 1, p. 107–123, [https://doi.org/10.1016/S0895-9811\(03\)00022-1](https://doi.org/10.1016/S0895-9811(03)00022-1).
- Hodnett, H.M., and Elliott, D.K., 2018, Carboniferous chondrichthyan assemblages from the Surprise Canyon and Watahomigani formations (latest Mississippian–Early Pennsylvanian) of the western Grand Canyon, Northern Arizona: *Journal of Paleontology*, v. 92, p. 1–33.
- Hoy, R.G., and Ridgeway, K.D., 2002, Syndepositional thrust-related deformation and sedimentation in an Ancestral Rocky Mountains basin, Central Colorado trough, Colorado, USA: *Geological Society of America Bulletin*, v. 114, no. 7, p. 804–828, [https://doi.org/10.1130/0016-7606\(2002\)114<0804:STRDAS>2.0.CO;2](https://doi.org/10.1130/0016-7606(2002)114<0804:STRDAS>2.0.CO;2).
- Irmis, R.B., Chure, D.J., Engelmann, G.F., Wiersma, J.P., and Lindström, S., 2015, The alluvial to eolian transition of the Chinle and Nugget formations in the southern Uinta Mountains, northeastern Utah, in Vanden Berg, M.D., Resselter, R., and Birgenheier, L.P., eds., *Geology of Utah's Uinta Basin and Uinta Mountains: Utah Geological Association Publication* 44, p. 13–48.
- Jessup, M.J., Jones, J.V., III, Karlstrom, K.E., Williams, M.L., Connelly, J.N., and Heizler, M.T., 2006, Three Proterozoic Orogenic Episodes and an Intervening Exhumation Event in the Black Canyon of the Gunnison Region, Colorado: *The Journal of Geology*, v. 114, p. 555–576, <https://doi.org/10.1086/506160>.
- Johnson, S.Y., 1987, Stratigraphic and sedimentological studies of late Paleozoic strata in the Eagle Basin and northern Aspen Sub-Basin, northwest Colorado: U.S. Geological Survey Open File Report 87-286, p. 1–83.
- Karlstrom, K.E., and Humphreys, E.D., 1998, Persistent influence of Proterozoic accretionary boundaries in the tectonic evolution of southwestern North America: Interaction of cratonic grain and mantle modification events: *Rocky Mountain Geology*, v. 33, no. 2, p. 161–179, <https://doi.org/10.2113/33.2.161>.
- Keller, G.R., and Hatcher, R.D., 1999, Some comparisons of the structure and evolution of the southern Appalachian-Ouachita orogen and portions of the Trans-European Suture Zone region: *Tectonophysics*, v. 314, p. 43–68, [https://doi.org/10.1016/S0040-1951\(99\)00236-X](https://doi.org/10.1016/S0040-1951(99)00236-X).
- Kent, D.V., and Irving, E., 2010, Influence of inclination error in sedimentary rocks on the Triassic and Jurassic apparent pole wander path for North America and implications for Cordilleran tectonics: *Journal of Geophysical Research: Solid Earth*, v. 115, p. 1–25, <https://doi.org/10.1029/2009JB007205>.
- Kimbrough, D.L., Grove, M., Gehrels, G.E., Dorsey, R.J., Howard, K.A., Lovera, O., Aslan, A., House, P.K., and Pearthree, P.A., 2015, Detrital zircon U-Pb provenance of the Colorado River: A 5 m.y. record of incision into cover strata overlying the Colorado Plateau and adjacent regions: *Geosphere*, v. 11, no. 6, p. 1719–1748, <https://doi.org/10.1130/GES00982.1>.
- Kissock, J.K., Finzel, E.S., Malone, D.H., and Craddock, J.P., 2018, Lower–Middle Pennsylvanian strata in the North American midcontinent record the interplay between erosional unroofing of the Appalachians and eustatic sea-level rise: *Geosphere*, v. 14, no. 1, p. 141–161, <https://doi.org/10.1130/GES01512.1>.
- Kluth, C.F., and Coney, P.J., 1981, Plate-tectonics of the Ancestral Rocky Mountains: *Geology*, v. 9, no. 1, p. 10–15, [https://doi.org/10.1130/0091-7613\(1981\)9<10:PTOTAR>2.0.CO;2](https://doi.org/10.1130/0091-7613(1981)9<10:PTOTAR>2.0.CO;2).
- Kolata, D.R., 2005, Bedrock geology of Illinois: Illinois State Geological Survey, scale 1:500,000.
- Kreisa, R.D., and Bambach, R.K., 1973, Environments of deposition of the Price Formation (lower Mississippian) in its type area, southwestern Virginia: *American Journal of Science*: Cooper, v. 273-A, p. 326–342.
- Kuiper, Y.D., and Hepburn, C., 2020, Detrital zircon populations of the eastern Laurentian margin in the Appalachians: *Geology*, v. 49, no. 2, p. 233–237.
- Lawton, T.F., 1994, Tectonic setting of Mesozoic sedimentary basins, Rocky Mountain region, United States, in Caputo, M.V., Peterson, J.A., and Franczyk, K.J., eds., *Mesozoic Systems of the Rocky Mountain Region, USA: Denver Colorado, Rocky Mountain Section, SEPM (Society for Sedimentary Geology)*, p. 1475–1506.
- Lawton, T.F., Buller, C.D., and Parr, T.R., 2015, Provenance of a Permian erg on the western margin of Pangea: Depositional system of Kunguria (late Leonardian) Castle Valley and White Rim sandstones and subjacent Cutler Group, Paradox, Utah, USA: *Geosphere*, v. 11, no. 5, p. 1–32, <https://doi.org/10.1130/GES01174.1>.
- Lawton, T.F., Cashman, P.H., Trexler, J.H., and Taylor, W.J., 2017, The late Paleozoic Southwestern Laurentian Borderland: *Geology*, v. 45, no. 8, p. 675–678.
- Lawton, T.F., Ruiz Urueña, J.E., Solari, L.A., Terrazas, C.T., Jauareze-Arriaga, E., and Ortega-Obregón, C., 2018, Provenance of Upper Triassic–Middle Jurassic strata of the Plomosas uplift, east-central Chihuahua, Mexico, and possible sedimentologic connections with Colorado Plateau depositional systems, in Ingersoll, R.V., Lawton, T.F., and Graham, S.A., eds., *Tectonics, Sedimentary Basins, and Provenance: A Celebration of the Career of William R. Dickinson: Geological Society of America Special Paper* 540, p. 481–507, [https://doi.org/10.1130/2018.2540\(22\)](https://doi.org/10.1130/2018.2540(22)).
- Lawton, T.F., Blakey, R.C., Stockli, D.F., and Liu, L., 2021, Late Paleozoic (Late Mississippian–Middle Permian) sediment provenance and dispersal in western equatorial Pangea: *Palaeogeography, Palaeoclimatology, Palaeoecology*, v. 572, p. 1–35, <https://doi.org/10.1016/j.palaeo.2021.110386>.
- Leary, R.J., Umhoefer, P., Smith, M.E., and Riggs, N., 2017, A three-sided orogen: A new tectonic model for Ancestral Rocky Mountain uplift and basin development: *Geology*, v. 45, no. 8, p. 735–738, <https://doi.org/10.1130/G39041.1>.
- Leary, R.J., Umhoefer, P., Smith, M.E., Smith, T.M., Saylor, J.E., Riggs, N., Burr, G., Lodes, E., Foley, D., Licht, A., Mueller, M.A., and Baird, C., 2020, Provenance of Pennsylvanian-Permian sedimentary rocks associated with the Ancestral Rocky Mountains orogeny in southwestern Laurentia: Implications for continental-scale Laurentian sediment transport systems: *Lithosphere*, v. 12, no. 1, p. 88–121, <https://doi.org/10.1130/L115.1>.
- Licht, A., Pullen, A., Kapp, P., Abell, J., and Giesler, N., 2016, Eolian cannibalism: Reworked loess and fluvial



- Geophysics, Geosystems, v. 18, p. 2872–2866, <https://doi.org/10.1002/2016GC006774>.
- Sundell, K.E., Gehrels, G.E., and Pecha, M.E., 2020, Rapid U-Pb geochronology by laser ablation multi-collector ICP-MS: Geostandards and Geoanalytical Research, v. 45, p. 37–57, <https://doi.org/10.1111/ggr.12355>.
- Suttner, L.J., and Dutta, P.K., 1986, Alluvial sandstone composition and paleoclimate, I. Framework mineralogy: Journal of Sedimentary Petrology, v. 56, no. 3, p. 329–345.
- Sweet, D.E., and Soreghan, G.S., 2010, Late Paleozoic tectonics and paleogeography of the ancestral Front Range: Structural, stratigraphic, and sedimentologic evidence from the Fountain Formation (Manitou Springs, Colorado): Geological Society of America Bulletin, v. 122, no. 3–4, p. 575–594, <https://doi.org/10.1130/B26554.1>.
- Sweet, D.E., Brotherton, J.J., Chowdhury, N.U.M.K., and Ramsey, C.E., 2021, Tectonic subsidence analysis of the Ancestral Rocky Mountains from the interior to the southern margin: Palaeogeography, Palaeoclimatology, Palaeoecology: Palaeoecology, v. 576, p. 1–16, <https://doi.org/10.1016/j.palaeo.2021.110508>.
- Thomas, W.A., 1991, The Appalachian-Ouachita rifted margin of southeastern North America: Geological Society of America Bulletin, v. 103, p. 415–431, [https://doi.org/10.1130/0016-7606\(1991\)103<0415:TAORMO>2.3.CO;2](https://doi.org/10.1130/0016-7606(1991)103<0415:TAORMO>2.3.CO;2).
- Thomas, W.A., Gehrels, G.E., and Romero, M.C., 2016, Detrital zircons from crystalline rocks along the Southern Oklahoma fault system, Wichita and Arbuckle Mountains, USA: Geosphere, v. 12, no. 4, p. 1224–1234, <https://doi.org/10.1130/GES01316.1>.
- Thomas, W.A., Gehrels, G.E., Lawton, T.F., Satterfield, J.I., Romero, M.C., and Sundell, K.E., 2019, Detrital zircons and sediment dispersal from the Coahuila terrane of northern Mexico into the Marathon foreland of the southern Midcontinent: Geosphere, v. 15, no. 4, p. 1102–1127, <https://doi.org/10.1130/GES02033.1>.
- Thomas, W.A., Gehrels, G.E., Sundell, K.E., Greb, S.F., Finzel, E.S., Clark, R.J., Malone, D.H., Hampton, B.A., and Romero, M.C., 2020, Detrital zircons and sediment dispersal in the eastern Midcontinent of North America: Geosphere, v. 16, no. 3, p. 817–843, <https://doi.org/10.1130/GES02152.1>.
- Thomas, W.A., Gehrels, G.E., Sundell, K.E., and Romero, M.C., 2021, Detrital-zircon analyses, provenance, and late Paleozoic sediment dispersal in the context of tectonic evolution of the Ouachita orogen: Geosphere, v. 17, no. 4, p. 1214–1247, <https://doi.org/10.1130/GES02288.1>.
- Trexler, J.H., Cashman, P.H., Snyder, W.S., and Davydov, V.I., 2004, Late Paleozoic tectonism in Nevada: Timing, kinematics, and tectonic significance: Geological Society of America Bulletin, v. 116, p. 525–538, <https://doi.org/10.1130/B25295.1>.
- Trudgill, B.D., 2011, Evolution of salt structures in the northern Paradox Basin: Controls on evaporite deposition, salt wall growth and supra-salt stratigraphic architecture: Basin Research, v. 23, p. 208–238, <https://doi.org/10.1111/j.1365-2117.2010.00478.x>.
- Vail, R.M.M., and Thompson, S., 1977, Seismic stratigraphy and global changes of sea level, Part 2: The depositional sequence as a basic unit for stratigraphic analysis, in Payton, C.E., ed., Seismic Stratigraphy: Applications to Hydrocarbon Exploration: American Association of Petroleum Geologists Bulletin Memoir, v. 26, no. 63, p. 57–62.
- Vermeesch, P., 2012, On the visualization of detrital age distributions: Chemical Geology, v. 312–313, p. 190–194, <https://doi.org/10.1016/j.chemgeo.2012.04.021>.
- Vermeesch, P., 2013, Multi-sample comparison of detrital age distributions: Chemical Geology, v. 341, p. 140–146, <https://doi.org/10.1016/j.chemgeo.2013.01.010>.
- Wang, W., and Bidgoli, T.S., 2019, Detrital zircon geochronologic constraints on patterns and drivers of continental-scale sediment dispersal in the Late Mississippian: Geochemistry, Geophysics, Geosystems, v. 20, p. 5522–5543, <https://doi.org/10.1029/2019GC008469>.
- Weber, B., Schaaf, P., Valencia, V.A., Iriondo, A., and Ortega-Gutiérrez, F., 2006, Provenance ages of late Paleozoic sandstones (Santa Rosa Formation) from the Maya block, SE Mexico: Implications on the tectonic evolution of western Pangea: Revista Mexicana de Ciencias Geológicas, v. 23, no. 3, p. 262–276.
- Weber, B., Valencia, V.A., Schaaf, P., Pompa-Mera, V., and Ruiz, J., 2008, Significance of Provenance Ages from the Chiapas Massif Complex (Southeastern Mexico): Redefining the Paleozoic Basement of the Maya Block and Its Evolution in a Peri-Gondwanan Realm: The Journal of Geology, v. 116, p. 619–639, <https://doi.org/10.1086/591994>.
- Webster, G.D., and Houck, K.J., 1998, Middle Pennsylvanian, late Atokan-early Desmoinesian echinoderms from an intermontane basin, the Central Colorado Trough: Journal of Paleontology, v. 72, p. 1054–1072, <https://doi.org/10.1017/S0022336000027402>.
- Whitmeyer, S.J., and Karlstrom, K.E., 2007, Tectonic model for the Proterozoic growth of North America: Geosphere, v. 3, no. 4, p. 220–259, <https://doi.org/10.1130/GES00055.1>.
- Willis, G.C., 1967, Influence of local structures on sedimentary cycles of Late Pennsylvanian beds of the Sacramento Mountains, Otero County, New Mexico, in Elam, J.G., and Chuber S., eds., Cyclic Sedimentation in the Permian Basin: Symposium of the West Texas Geological Society, Midland, Texas, 19–20 October, p. 100–110.
- Wissink, G.K., Hoke, G.D., Garzzone, C.N., and Liu-Zeng, J., 2016, Temporal and spatial patterns of sediment routing across the southeast margin of the Tibetan Plateau: Insights from detrital zircon: Tectonics, v. 35, p. 2538–2563, <https://doi.org/10.1002/2016TC004252>.
- Yang, K., and Dorobek, S.L., 1995, The Permian Basin of the west Texas and New Mexico: Flexural modeling and evidence for lithospheric heterogeneity across the Marathon foreland, in Dorobek, S.L., ed., Stratigraphic Evolution of Foreland Basins: Society of Economic Petroleum Memoir Special Publication, no. 52, p. 37–50, <https://doi.org/10.2110/pec.95.52.0037>.
- Ye, H., Royden, L., Burchfield, C., and Schuepbach, M., 1996, Late Paleozoic deformation of interior North America: The Greater Ancestral Rocky Mountains: AAPG Bulletin, v. 80, no. 9, p. 1397–1423.

SCIENCE EDITOR: WENJIAO XIAO  
ASSOCIATE EDITOR: TIMOTHY KUSKY

MANUSCRIPT RECEIVED 13 AUGUST 2021  
REVISED MANUSCRIPT RECEIVED 28 AUGUST 2022  
MANUSCRIPT ACCEPTED 25 OCTOBER 2022

Printed in the USA